Chapter: 3

Location of MPB and Room Temperature Crystal Structure of BMT-PT and BMZ-PT

Chapter-3

3.1 Introduction

In this chapter we have investigated the crystal structure of (1-x)$Bi(Mg_{1/2}Ti_{1/2})O_3$-x$PbTiO_3$ [BMT-PT] and (1-x)$Bi(Mg_{1/2}Zr_{1/2})O_3$-x$PbTiO_3$ [BMZ-PT] ceramics across morphotropic phase boundary (MPB). Rietveld structure refinement of the XRD patterns of various compositions across MPB have been done to determine the crystal structure and location of the MPB. In case of (1-x)$Bi(Mg_{1/2}Ti_{1/2})O_3$-x$PbTiO_3$ [BMT-PT] and (1-x)$Bi(Mg_{1/2}Zr_{1/2})O_3$-x$PbTiO_3$ [BMZ-PT] there is controversy about the structure and location of the morphotropic phase boundary compositions. Many authors have reported that the structure of MPB is the coexistence of the rhombohedral and tetragonal phases, while some authors have reported that the structure as coexistence of pseudocubic and tetragonal structures [Chen et al. (2009); Zhang et al. (2010); Shabbir et al. (2007); Qureshi et al. (2007)]. Randall et al. (2004) have reported the phase diagram of BMT-PT using the results of temperature dependent dielectric studies, piezoelectric coefficient and room temperature XRD data. These authors have reported a phase transition from pseudocubic/rhombohedral (space group R3m) to tetragonal (space group P4mm) structure with changing composition. The MPB is reported to lie around x=0.37 [Randall et al. (2004)]. Similarly, in case of the BMZ-PT, Qureshi et al. (2007) have reported the phase diagram using the results of temperature dependent dielectric studies, impedance data and room temperature XRD data. They have reported a phase transition from ferroelectric rhombohedral (space group R3m) to ferroelectric tetragonal

(space group P4mm) with changing composition. The MPB is reported to lie around x=0.55 [Qureshi et al. (2004)]. However, XRD patterns reported by these authors do not reveal any splitting corresponding to rhombohedral structure. Further, no detailed Rietveld structural analysis has been done for BMT-PT and BMZ-PT solid solutions to precisely determine the structural parameters and the structure of the MPB phase. The structure and the location of the MPB for BMT-PT and BMZ-PT needs to be resolved, by Rietveld structural analysis of these materials, for better understanding of structure property correlations.

In this Chapter, we have resolved controversies regarding the crystal structure and location of the MPB in BMT-PT and BMZ-PT at room temperature. We have refined the room temperature crystal structure of BMT-PT and BMZ-PT solid solution across morphotropic phase boundary region in the composition range of $0.28 \leq x \leq 0.45$ and $0.55 \leq x \leq 0.61$ respectively using Rietveld refinement method. We find a monoclinic phase (space group Pm) in the MPB region for the BMT-PT solid solution, while coexistence of tetragonal and cubic structure for the BMZ-PT solid solution. We have also determined precisely the stability region of various crystallographic phases around the MPB at room temperature for both the BMT-PT and BMZ-PT solid solutions.

3.2 Experimental details

The samples used for the present work were prepared by solid state ceramic rout as described in Chapter 2. For the XRD characterization, sintered pellets were crushed into fined powders and then annealed at 500^{o}C for 12 hours to remove the strains introduced during crushing. The microstructure of the

sintered sample surface was studied by Scanning electron microscope (SEM) using ZEISS SUPRA40. Thin gold film of the order of few nanometre was coated on the sintered pellets before examining under SEM. X-ray diffraction measurements were carried out using an 18kW rotating anode Cu based Rigaku powder diffractometer operating in the Bragg-Brentano geometry and fitted with graphite monochromator in the diffracted beam line.

The structural refinements were carried out by using Rietveld method [Carvajal (2001), (2011)]. In the Rietveld method of structural refinement, the difference between the experimental and theoretical XRD profiles is minimized in the least squares sense to get the satisfactory fit. For two competing structures, the structural model with better fit and lower χ^2 value is accepted. The Rietveld method also gives the most precise estimate of the relative phase fraction of the coexisting phases. Rietveld refinement of the structures was carried out by using FULLPROF suite [Carvajal (2001), (2011)]. Sixth coefficient polynomial was used to define the background. Pseudo-Voigt function was used to define profile shape. We fixed the occupancy parameters of all the ions at the nominal composition during refinement. Isotropic thermal parameter was used for all the ions except A-site cations for which the anisotropic thermal parameters were used due to high value of isotropic thermal parameters. The details of the Rietveld refinement are given in the next section.

3.3 Details of Rietveld refinement method

The structure determination of the powder diffraction data is not an easy job because in powder diffraction data the three dimensional crystallographic

information in reciprocal space is collapsed into one dimension i.e. Bragg's angle. Therefore Rietveld developed a method of least square refinement in which the powder XRD data of the sample and theoretically calculated data gives the best fit as a whole for the crystal structure, instrumental factor, diffraction optics effects etc. The Rietveld refinement technique is essential for refinement of the appropriate structure using powder diffraction data. The parameter called the residual (S_y) is required to be minimized in the least square refinement [Young (1996)]. The S_y is the weighted sum of squared differences between the observed and calculated intensity values at the i^{th} step of the XRD pattern:

$$S_y = \sum W_i(Y_i - Y_{ci})^2 \quad \ldots\ldots\ldots\ldots\ldots\ldots 3.1$$

Where, Y_i is the observed intensity and Y_{ci} is the theoretically calculated intensity at the i^{th} step and W_i is a suitable weight given by $W_i = (Y_i)^{-1}$, and the sum is for all data points.

The Rietveld refinement method adjust the refinable parameters until the residual (eqn 3.1) is minimized. That is called the "best fit" of the theoretically calculated and the observed pattern of the XRD data. The Rietveld method have developed several R-values that are now commonaly used in Rietveld refinement. The following R-values measure the goodness of the fit, which are commonly used to check the correctness of the refined structure [Young (1996)].

(i) R-structure factor : $R_F = \frac{\sum |(I_k(\prime obs\prime))^{1/2} - (I_k(calc)^{1/2})|}{\sum (I_k(\prime obs\prime))^{1/2}}$

(ii) R-Bragg factor : $R_B = \frac{\sum |I_k(\prime obs\prime) - I_k(calc)|}{\sum (I_k(\prime obs\prime))}$

(iii) R-pattern : $R_P = \frac{\sum |Y_i(obs) - Y_i(calc)|}{\sum Y_i(obs)}$

(iv) R-weighted pattern : $R_{WP} = \left\{\frac{\sum W_i(Y_i(obs)-Y_i(calc))^2}{\sum W_i Y_i(obs)^2}\right\}^{1/2}$

(v) R-expected : $R_e = \left[\frac{(N-P)}{\sum W_i Y_i(obs)^2}\right]^{1/2}$

Where, I_k is the intensity assigned to the k^{th} Bragg reflection at the end of the refinement cycle. The N and P, are the number of the observations and variables respectively. The Bragg intensity, I_k is rarely observed directly. The value of I_k are obtained from programmatic allocation of the total observed intensity in a scramble of overlapped reflection to the individual reflections, according to the ratios of those reflection intensities in the calculated pattern.

The goodness of the fit (S) can be obtained from the expected and weighted pattern of R-factors

$$S = \frac{R_{WP}}{R_e} = \left[\frac{S_y}{(N-P)}\right]^{1/2} \quad \text{……..……} \quad (3.2)$$

The value of S also depends on the quality of powder diffraction data and is only an indicator of the global minimum solution. The S is the main parameter for the confirming the fit. Irrespective of the S value, one seeks to achieve a difference patterns as flat as possible before confirming a model. The goodness of the fit for the system is often represented by an indicator called χ^2 which is defined as:

$$\chi^2 = S^2 = \left[\frac{R_{WP}}{R_e}\right]^2 = \left[\frac{S_y}{(N-P)}\right] \quad \text{…….. (3.3)}$$

Thus the R_{wp} is the most meaningful agreement factor among all the agreement factor for the checking the convergence of the refimement and R_e is for the data

quality. The value of R_{wp} and R_e should be as low as possible for the accurate structure parameters. The other refinable parameters in the Rietveld refinement technique includes structural parameters (such as positional coordinates, unit cell parameters, thermal parameters etc.), sample parameters (such as stain, domain size, preferred orientation, etc.), Instrumental parameters (FWHM of the peaks due to the diffraction geometry, shift of the origin, background etc.) and the scale factor [Young (1996)].

The shape of the powder diffraction reflection is influenced by both the sample and instrument. They vary as a function of two theta [Young (1996)]. In the Rietveld structure refinements among the various peak shape functions, the pseudo-Voigt i.e. an approximation of the Voigt function, is most widely used. It is nothing but the linear combination of Lorentzian (L) and Gaussian (G) component in the ratio defined as:

$$pV(x)= \eta L(x) + (1- \eta)G(x) \qquad \ldots\ldots\ldots\ldots\ldots\ldots \quad (3.4)$$

Where, η is the pseudo-Voigt mixing parameter. The value of χ^2 should never be less than one for the refinement of powder diffraction data. This may be because of the fact that standard uncertainties for the data are overestimated or additional parameters have been introduced so that the model is fitting the noise. Such types of features are common in powder diffraction [Toby (2006)]. However, if $\chi^2 >> 1$, then the model is logical but the standard uncertainty values are underestimated or it may be because of the model is imperfect, because there are errors in the data that do not correspond to the model or finally the model is incorrect [Toby (2006)]. If the values of χ^2 is nearly equal to 1 it does not mean that the fit is

correct. This may be achieved by taking different models which can give equivalent fits due to insufficient experimental data [Toby (2006)]. The peak shape functions for all the peaks contain half width of the Bragg peaks or the full width at half maxima (FWHM) whose angular dependence is expressed by the famous Coglioti function [Caglioti et al. (1958)]:

$$FWHM = U\tan^2\theta + V\tan\theta + W \qquad \ldots\ldots\ldots\ldots\ldots \quad (3.5)$$

Where, U, V and W are half width parameters which is also refinable parameters to achieve the best fit between the observed and theoretically calculated profile.

3.4 Details of the Rietveld refinement of BMT-PT and BMZ-PT

The Rietveld structure analysis were carried out by using FULLPROF package [Carvajal (2001), (2011)]. For the Rietveld refinement, background was modelled using sixth order polynomial while the Pseudo-Voigt function has been selected to generate profile shape for the peaks. The occupancy parameters for all the ions were fixed at nominal composition during refinement. All the other parameters such as background, zero correction, scale factor, half width parameters (U, V and W), lattice parameters, positional coordinates and thermal parameters were varied during the refinement. The isotropic thermal parameter were used during refinement for all the atoms but for A-site i.e. Pb/Bi ions, the isotropic thermal parameter was very high. Therefore, we have considered the anisotropic thermal parameters for A-site cations (Pb/Bi) for all the compositions of BMT-PT and BMZ-PT piezoceramics. It resulted in better fit for the refinement. The anisotropic peak shape function suggested by Stephens (1999)

and also incorporated in the Fullprof program was used to refine the structure of the powder diffraction data.

The Wyckoff positions and asymmetric unit for the various space groups used for the Rietveld refinement of various structures of BMT-PT and BMZ-PT system in the present work are given below:

(i) In the cubic structure with Pm3m space group, the occupancy of Bi/Pb ions were fixed at 1(a) sites (0, 0, 0), Ti/Zr ions at 1(b) sites (1/2, 1/2, 1/2) and oxygen ions at 3(c) sites (1/2, 1/2, 0).

(ii) For the refinement of the rhombohedral structure with space group R3m, we used the hexagonal unit cell having lattice parameters $a_H=b_H=\sqrt{2}a_R$ and $c_H=\sqrt{3}a_R$, where a_R corresponds to rhombohedral lattice parameter. To fix the origin for the rhombohedral structure, the z-coordinate of O ion was fixed at 0.167. In the asymmetric unit of the rhombohedral structure with R3m space group, Bi/Pb and Ti/Zr/Mg ions occupy 3(a) sites at (0, 0, z) and O ion at the 9(b) site at (x, 2x, z).

(iii) In the tetragonal structure with P4mm space group, the occupancy of Bi/Pb ions were fixed at 1(a) sites (0, 0, z), Ti/Mg/Zr and O_I in 1(b) sites at (1/2, 1/2, z), and O_{II} in 2(c) sites at (1/2, 0, *z*).

(iv) For the monoclinic structure with space group Cm, the occupancy of Bi/Pb, Ti/Mg/Zr and O_I were fixed in 2(a) sites at (x, 0, z) and O_{II} in 4(b) sites at (x, y, z).

(v) For the monoclinic structure with space group Pm, the occupancy of Bi/Pb and O_I ions were fixed in 1(a) sites at (x, 0, *z*), Ti/Mg/Zr, O_{II} and O_{III} in 1(b) sites at (x, 1/2, *z*).

For the analysis of the structure in this chapter we have shown in figures Rietveld fit for some selected pseudocubic reflections, but in all these cases Rietveld refinement is performed for the entire range of the pattern i.e. $2\theta=20^o$ to 120^o.

3.5 Results and discussion

3.5.1 Crystal structure and location of MPB in BMT-PT at room temperature

The room temperature X-ray diffraction patterns of the BMT-PT ceramics sintered at 950^{o}C for the compositions with x=0.28, 0.30, 0.31, 0.32, 0.33, 0.34, 0.35, 0.36, 0.37, 0.38, 0.40, and 0.45 are shown in Fig. 3.1. As can be seen from Fig. 3.1, pure perovskite phase is obtained for all the compositions, except some weak impurity reflections, for the composition x=0.28. Appearance of non-perovskite phases is expected for the lower compositions, since one of the component BMT does not crystallize into perovskite structure under usual synthesis conditions. Appearance of impurity phases for lower compositions is reported by earlier workers also [Zhang et al. (2011)]. For the perovskite phase of x=0.28, the diffraction pattern could be indexed by using pseudocubic structure. For the composition with x=0.45, the characteristic splitting of the tetragonal structure is observed, as all the peaks could be indexed by considering tetragonal unit cell for perovskite structure.

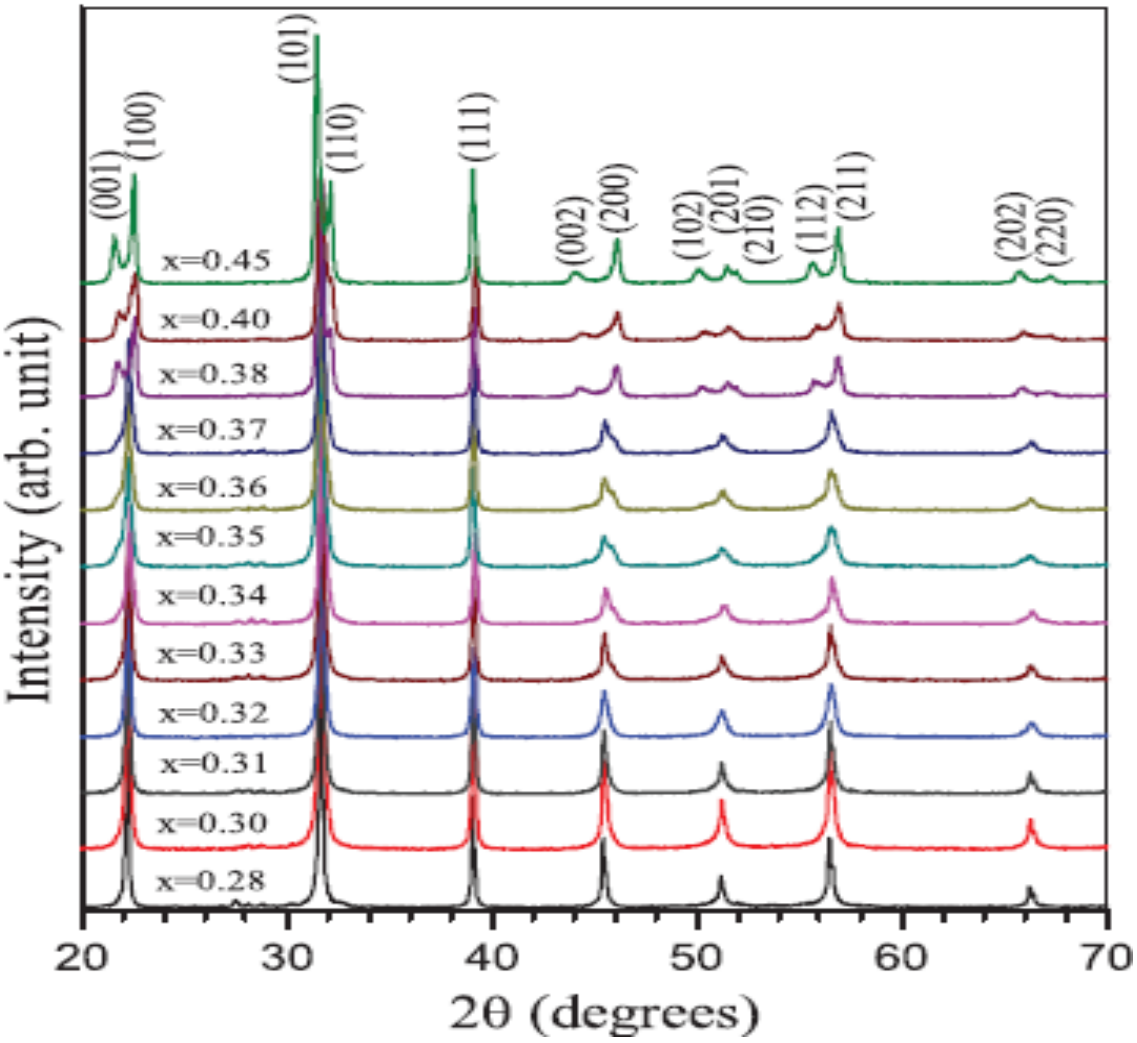

Fig.3.1 Powder x-ray diffraction patterns of BMT-PT piezoceramics with compositions x=0.28, 0.30, 0.31, 0.32, 0.33, 0.34, 0.35, 0.36, 0.37, 0.38, 0.40, and 0.45, sintered at 950ºC.

To analyse the structure intermediate compositions we show in Fig. 3.2, zoomed pseudocubic (110), (111), and (200) XRD profiles for various compositions of BMT-PT. We have removed the $K_{\alpha 2}$ component in all these profiles using standard software. For the composition range $0.28 \leq x \leq 0.31$, the peaks corresponding to pseudocubic reflections (110), (111), and (200) appear to be singlet suggesting pseudocubic structure. For $x \geq 0.32$, the width of the (110) and (200) peaks increases significantly, eventually leading to asymmetric tails on the higher and lower two-theta sides, which become more prominent for the compositions with x=0.35, 0.36, and 0.37. The pseudocubic (200) profile shows triplet character for these compositions signifying presence of a low symmetry monoclinic phase or coexistence of the two phases. The morphotropic phase boundary region exists in this composition range. It will be shown in Section 3.5.3, using Rietveld analysis of the X-ray diffraction data that the structure in the composition range $0.35 \leq x \leq 0.40$ consists of coexisting tetragonal (P4mm) and monoclinic (Pm) phases. For the compositions with $x > 0.37$, the diffraction profiles show splitting similar to that for x=0.45, suggesting predominantly tetragonal structure. As discussed in Section 3.5.4, Rietveld refinement of the structure confirms that the dominant phase is tetragonal with space group P4mm in these compositions.

3.5.2 Monoclinic structure with space group Pm (x=0.32)

The room temperature structure of BMT-PT composition with x=0.32 is reported to be rhombohedral by earlier authors [Randall et al. (2004); Zhang et al. (2011)].

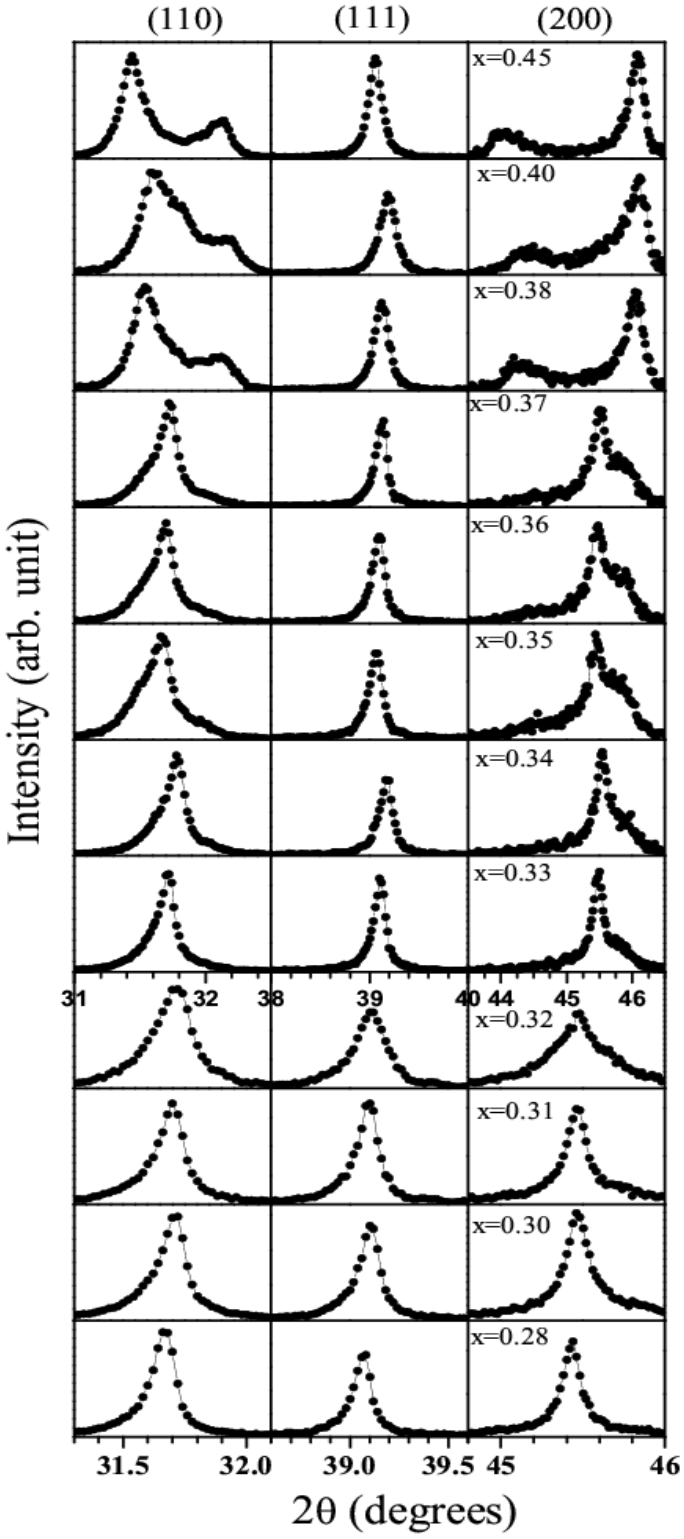

Fig.3.2 Evolution of the XRD profiles of the pseudocubic (110), (111) and (200) reflections (corresponding to Cu $K_{\alpha 1}$ radiation) for various compositions of BMT-PT at room temperature.

We show here that the rhombohedral structure in the R3m space group could not account for the observed x-ray diffraction profiles. In view of this, we have considered the monoclinic structure with space group Pm and Cm in structure refinement from Rietveld refinement method, which have been observed in the morphotropic phase boundary region of several MPB ceramics [Singh et al. (2001), (2003), (2005), (2006), (2008); Kiat et al. (2002); Pandey et al. (2008), (2014)]. Fig. 3.3 shows the experimentally observed, Rietveld calculated, and their difference profiles for pseudocubic (110), (111), and (200) reflections, along with the agreement factors, using different space groups. The structure refinement was performed using complete XRD pattern in the two theta range 20 to 120 degrees. Mismatch between the Rietveld calculated and observed profiles for the pseudocubic (111), and (200) reflections is large in case of the space group R3m, and therefore it is rejected. The fit between the observed and Rietveld calculated profiles is very good in case of the monoclinic phase with space group Pm. The values of χ^2 are 2.80, 2.42, and 1.95 for the space groups R3m, Cm, and Pm, respectively. The lowest value of χ^2 for Pm space group confirms the monoclinic structure for the composition with x=0.32. Rietveld fit for the full pattern, using monoclinic structure with space group Pm, for the composition with x=0.32 is shown in Fig. 3.4. The overall fit is quite satisfactory. Thus, the structure of BMT-PT with x=0.32 is monoclinic in the Pm space group. The refined structural parameters are given in Table 3.1. The structure of the compositions with x=0.31, 0.30, and 0.28, where no clear splitting is observed, was refined by cubic (Pm3m) and rhombohedral (R3m) structures.

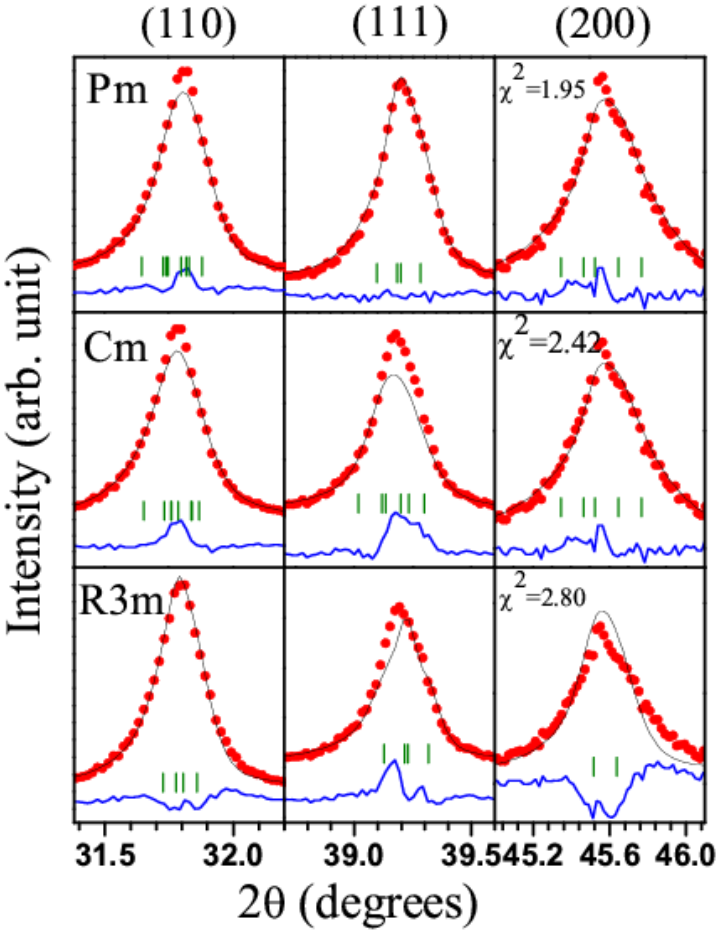

Fig.3.3 Experimentally observed (dots), Rietveld calculated (continuous line) and their difference (continuous bottom line) XRD profiles obtained after Rietveld analysis of the powder XRD data for pseudocubic (110), (111), and (200) reflection of $0.68Bi(Mg_{1/2}Ti_{1/2})O_3$-$0.32PbTiO_3$ using monoclinic (Pm), monoclinic (Cm) and rhombohedral (R3m) structures. The vertical tick-marks above the difference plot show the peak positions.

Table 3.1: Refined structural parameters of 0.68BMT-0.32PT ceramics, using monoclinic space group Pm.

x (space group)	Ions	x	y	z	Thermal parameters ($Å^2$)	Lattice Parameters (Å)
0.32	Bi/Pb	0.0	0.0	0.0	β_{11}=0.036(6),β_{22}=0.109(9),	a_M=3.9801(5)
					β_{33}=0.010(4)	b_M=3.9726(1)
(Pm)	Mg/Ti	0.508(1)	0.5	0.564(1)	Biso=0.150(3)	c_M=3.9965(3)
	O_I	0.467(1)	0.0	0.55(2)	Biso=0.068(2)	β=90.181(2)°
	O_{II}	0.441(1)	0.5	0.173(6)	Biso=0.190(5)	
	O_{III}	-0.03(4)	0.5	0.563(2)	Biso=0.61(1)	

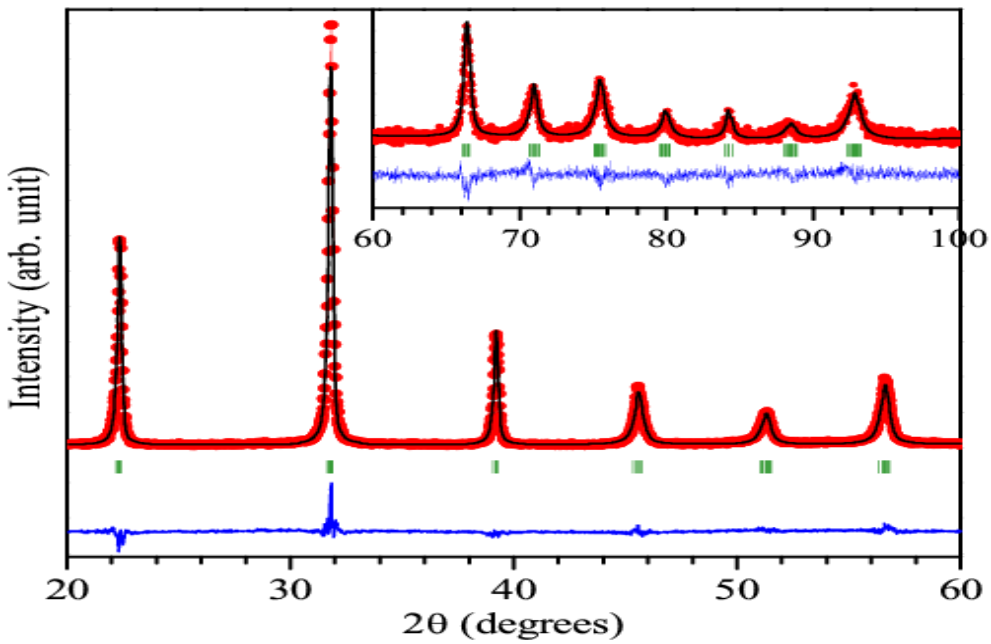

Fig.3.4 Experimentally observed (dots), Rietveld calculated (continuous line) and their difference (continuous bottom line) profiles obtained after Rietveld analysis of the powder XRD data for 0.68Bi($Mg_{1/2}Ti_{1/2}$)O_3-0.32$PbTiO_3$ using monoclinic (Pm), structures. The vertical tick-marks above the difference plot show the peak positions.

A careful analysis of the fit suggests that both the structures did not give the satisfactory fit between experimentally observed and Rietveld calculated XRD profiles. Consideration of monoclinic structure with Pm space group gives the better fit and lower χ^2 value. Thus, we can conclude that the structure of the pseudocubic compositions is short range monoclinic in Pm space group for these compositions. It will be shown in chapter 4, that the application of high electric field poling transforms the short range monoclinic structure into long range monoclinic structure in the Pm space group, with clear splitting in the diffraction profiles.

3.5.3 Phase coexistence with space groups "Pm+P4mm" (x=0.35)

The diffraction profiles of the BMT-PT compositions with $0.35 \leq x \leq 0.37$ shown in Fig. 3.2 exhibit clear splitting, characteristic of the phase coexistence, suggesting them to lie in the MPB region. Since the structure of the composition with x=0.32 is monoclinic in Pm space group and the compositions on the $PbTiO_3$ side of the MPB have tetragonal structure with P4mm space group, it is expected that these two phases will coexist in the MPB region. However, since earlier researchers [Chen et al. (2009); Zhang et al. (2010)] reported coexistence of rhombohedral and tetragonal structures in the MPB region, we also considered this structural model in the structure refinement. In Fig. 3.5, we show the Rietveld fit for the pseudocubic (110), (111), and (200) profiles, for the composition with x=0.35, using coexisting "R3m+P4mm" and "Pm+P4mm" structures. As can be seen from Fig. 3.5, the coexistence of rhombohedral and tetragonal structures could not account well the observed diffraction profiles,

particularly for the pseudocubic (111) and (200). However, the coexistence of "Pm+P4mm" structures gives significantly better fit. The value of χ^2 is 2.01 and 1.85 for the coexisting "R3m+P4mm" and "Pm+P4mm" structures, respectively, favouring the later. The Rietveld refinement of the structure for other compositions in the MPB region also confirms the coexistence of "Pm+P4mm" structures. The Rietveld fit for the full XRD pattern, using coexisting monoclinic and tetragonal structures with space group Pm and P4 mm, for the composition with x=0.35 is shown in Fig. 3.6. The overall fit is very good. The refined structural parameters are given in Table 3.2.

Table 3.2: Refined structural parameters of 0.65BMT-0.35PT ceramics, using monoclinic space group Pm and tetragonal space group P4mm.

x (space group)	Ions	x	y	z	Thermal parameters (Å^2)	Lattice Parameters (Å)
0.35	Bi/Pb	0.0	0.0	0.0	β_{11}=0.11(2),β_{22}=0.13(2), β_{33}=0.07(2)	a_M=3.9819(4) b_M=3.9675(3)
(Pm)	Mg/Ti	0.516(5)	0.5	0.55(2)	Biso=0.37(3)	c_M=4.0026(2)
	O_I	0.46(5)	0.0	0.57(5)	Biso=0.41(5)	β=90.232(4)°
	O_{II}	0.49(8)	0.5	0.18(4)	Biso=0.72(2)	
	O_{III}	-0.05(2)	0.5	0.58(4)	Biso=0.276(7)	a_T=3.9465(4)
(P4mm)	Bi/Pb	0.0	0.0	0.0	β_{11}=β_{22}=0.048(7), β_{33}=0.013(4)	c_T=4.0688(2)
	Mg/Ti	0.5	0.5	0.55(1)	Biso=0.948(7)	
	O_I	0.5	0.5	0.15(4)	Biso=0.813(6)	
	O_{II}	0.5	0.0	0.59(1)	Biso=0.970(8)	

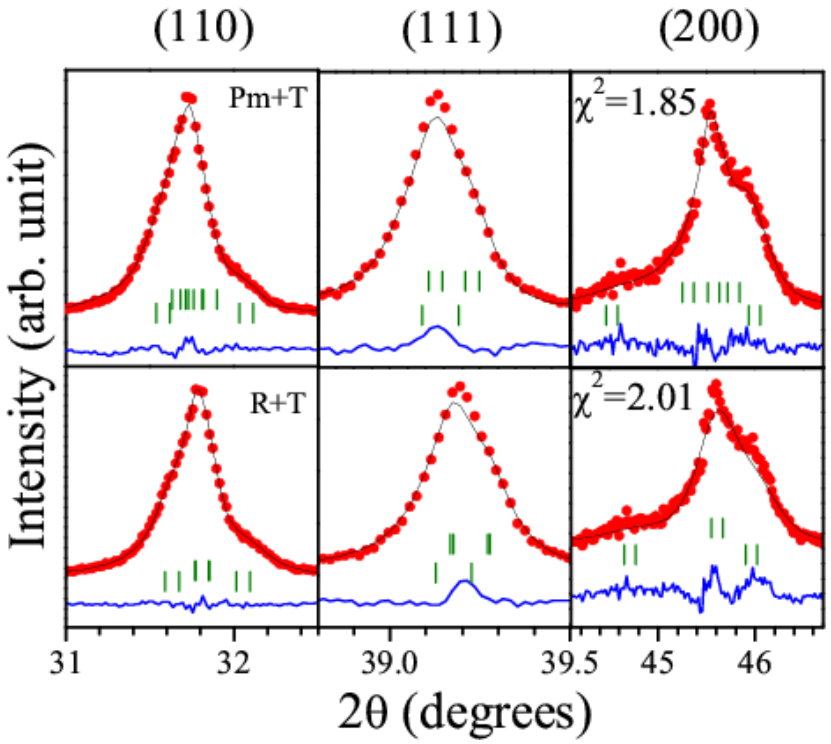

Fig.3.5 Experimentally observed (dots), Rietveld calculated (continuous line) and their difference (continuous bottom line) profiles obtained after Rietveld analysis of the powder XRD data for pseudocubic (110), (111), and (200) reflections of $0.65Bi(Mg_{1/2}Ti_{1/2})O_3$-$0.35PbTiO_3$ using monoclinic+tetragonal (Pm+P4mm) and rhombohedral+tetragonal (R3m+P4mm) structures. The vertical tick-marks above the difference plot show the peak positions.

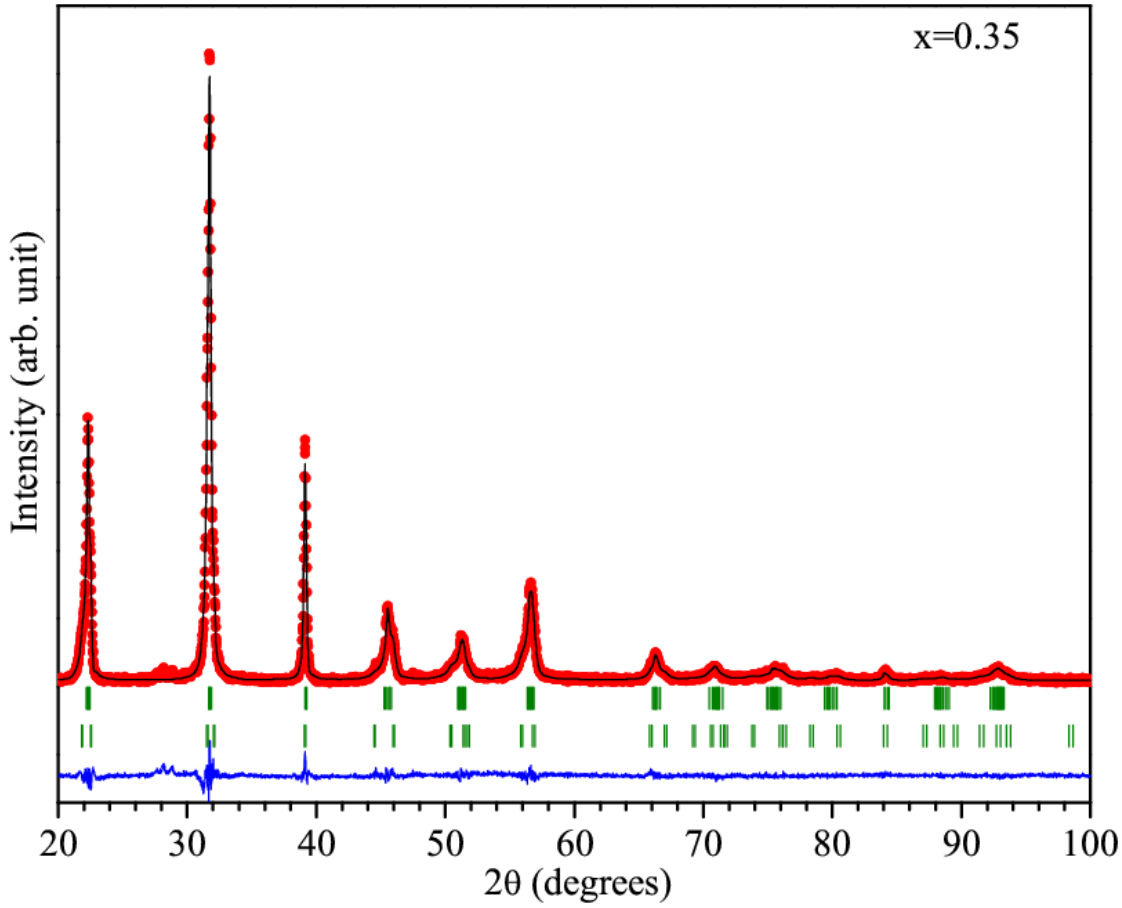

Fig.3.6 Experimentally observed (dots), Rietveld calculated (continuous line) and their difference (continuous bottom line) profiles obtained after Rietveld analysis of the powder XRD data for $0.65Bi(Mg_{1/2}Ti_{1/2})O_3$-$0.35PbTiO_3$ using monoclinic+tetragonal (Pm+P4mm), structures. The vertical tick-marks above the difference plot show the peak positions.

3.5.4 Tetragonal structure with space group P4mm (x=0.45)

The structure of the composition with x=0.45 was refined by considering tetragonal phase in the space group P4mm and the fit is shown in Fig. 3.7. Broadly, the diffraction profiles could be satisfactory accounted by the tetragonal structure. However, mismatch is seen for the diffuse scattering contribution in between the tetragonal reflections. As reported for the tetragonal compositions close to MPB, in PZT [Noheda et al. (1999)], and PMN-PT [Singh et al. (2003)] ceramics, consideration of coexisting monoclinic phase improves the fit. The refined structural parameters and various agreement factors for the composition with x=0.45 using tetragonal (P4mm) structure are given in Table 3.3.

Table 3.3: Refined structural parameters of 0.55BMT-0.45PT ceramics using tetragonal space group P4mm.

x (space group)	Ions	x	y	z	Thermal parameters ($Å^2$)	Lattice Parameters (Å)
0.45	Bi/Pb	0.0	0.0	0.0	$\beta_{11}=\beta_{22}=0.049(6)$, $\beta_{33}=0.028(7)$	$a_T=3.9483(1)$ $c_T=4.0962(3)$
(P4mm)	Mg/Ti	0.5	0.5	0.55(2)	$B_{iso}=0.821(2)$	
	O_I	0.5	0.5	0.13(3)	$B_{iso}=0.934(4)$	
	O_{II}	0.5	0.0	0.54(1)	$B_{iso}=0.50(1)$	

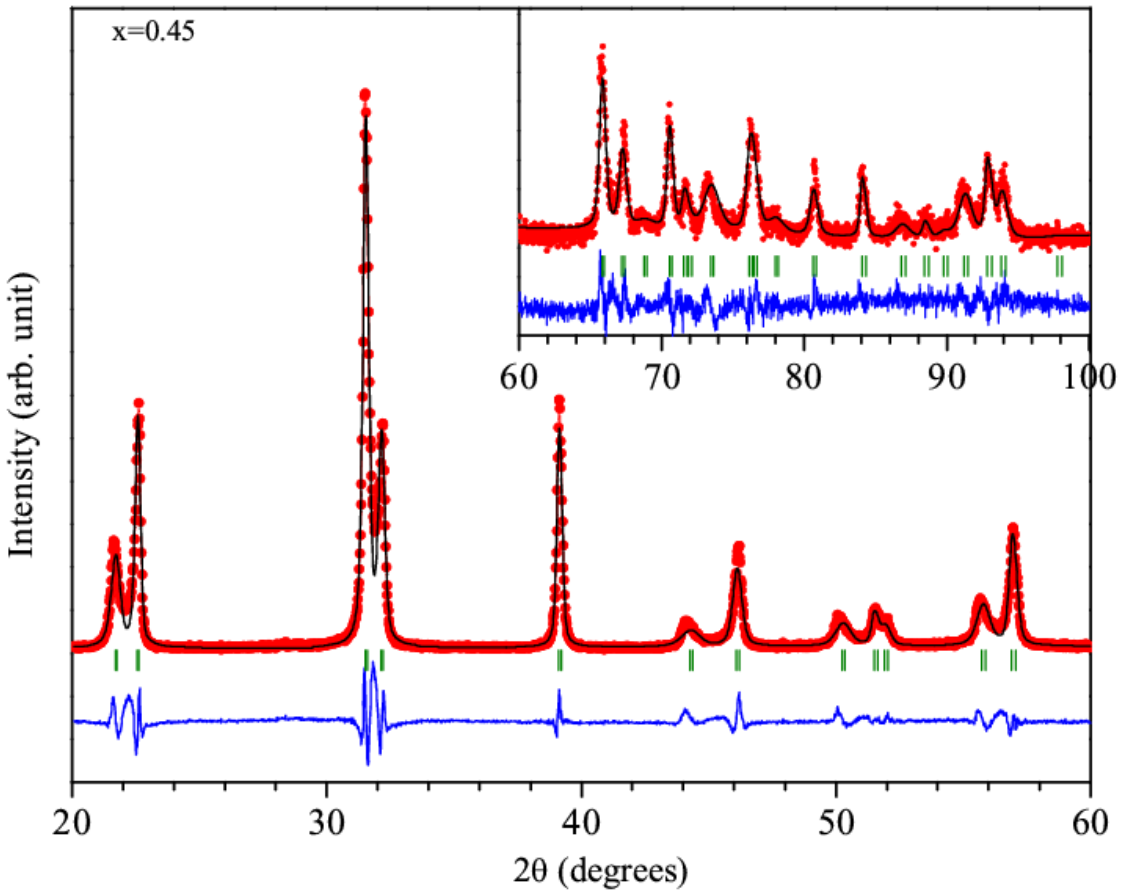

Fig.3.7 Experimentally observed (dots), Rietveld calculated (continuous line) and their difference (continuous bottom line) profiles obtained after Rietveld analysis of the powder XRD data for $0.55Bi(Mg_{1/2}Ti_{1/2})O_3$-$0.45PbTiO_3$ using tetragonal (P4mm) structure. The vertical tick-marks above the difference plot show the peak positions.

3.5.5 Variation of lattice parameters and phase fractions with composition for BMT-PT

Variation of lattice parameters with composition (x) for BMT-PT in the composition range $0.28 \leq x \leq 0.40$ is shown in Fig. 3.8. The monoclinic lattice parameters are denoted by a_M, b_M, and c_M. The monoclinic angle is denoted by β. The tetragonal lattice parameters are denoted by a_T and c_T. As shown in Fig. 3.8, the a_M and b_M parameters decrease slightly with increasing the PT concentration but the c_M parameter shows increasing trend. As expected while moving to PT side, the a_T parameter decreases, while the c_T parameter increases continuously, with increasing the composition (x). The monoclinic angle β shows increasing trend up to the composition x=0.37 and then decreases. Variation of the monoclinic phase fraction with PT concentration, in the composition range $0.33 \leq x \leq 0.40$, is shown in Fig. 3.9. As expected, the fraction of monoclinic phase linearly decreases with increasing PT concentration. The phase fractions of the monoclinic and tetragonal compositions are nearly equal around the MPB composition [see Fig. 3.9], where maximum piezoelectric response is obtained.

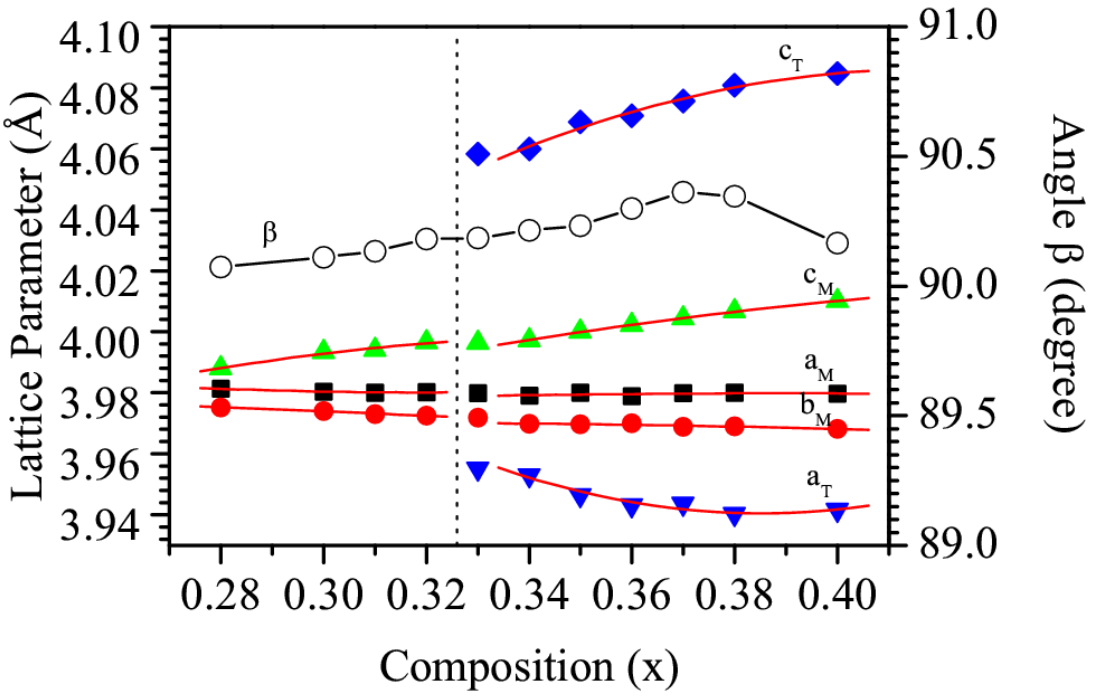

Fig.3.8 Variation of lattice parameters with composition for BMT-PT ceramics.

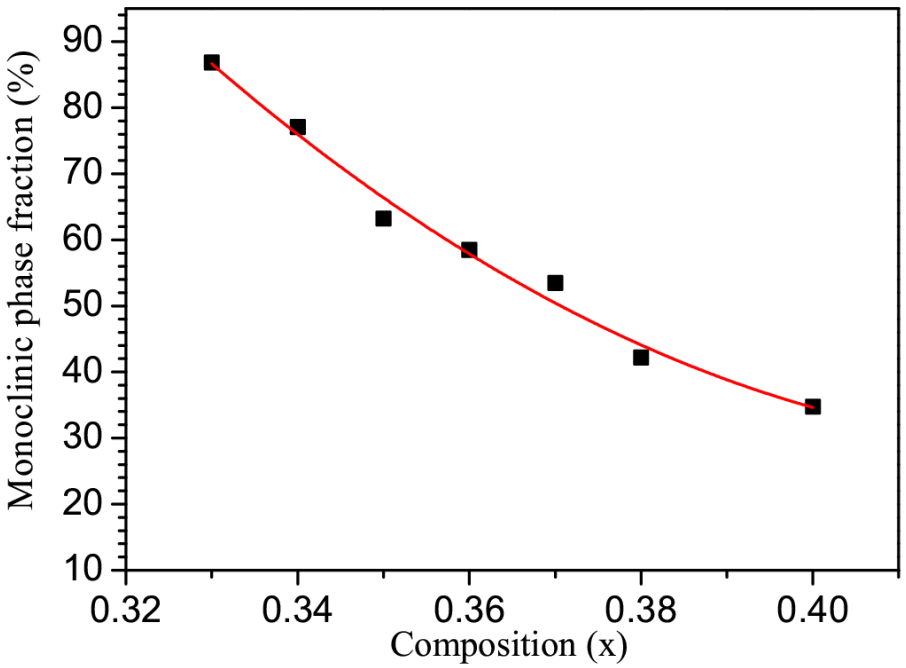

Fig.3.9 Variation of monoclinic phase fraction with composition for BMT-PT ceramics.

3.6 Grain size dependent phase stabilities in BMT-PT

In forgoing sections of this chapter we have shown that phase stability at room temperature in BMT-PT is dependent on the composition. Now we will show that crystallographic phases around MPB in BMT-PT can be significantly affected by changing particle size. The results of structural analysis for sample of various particle sizes for composition with x=0.35 are presented in subsequent sections.

3.6.1 Evolution of Crystal structure with varying heat treatment in 0.65BMT-0.35PT

The X-ray diffraction patterns for BMT-PT piezoceramics heat treated at various temperatures for the composition with x=0.35 are shown in Fig. 3.10. As can be seen from Fig. 3.10 the shape of the XRD profiles changes with varying the heat treatment temperature from 850^{o}C to 1000^{o}C. Fig. 3.11 shows the selected pseudocubic (110), (111) and (200) profiles for 0.65BMT-0.35PT piezoceramics at various heat treatment temperature. The contribution from the $CuK_{\alpha 2}$ wavelength is also present, for all the profiles shown in Fig. 3.11. As can be seen from Fig. 3.11, with decreasing heat treatment temperature the (110) and (200) profiles show enhanced broadening and development of asymmetric hump and new peaks. This suggests that the structure is changing with decreasing heat treatment temperature/particle size.

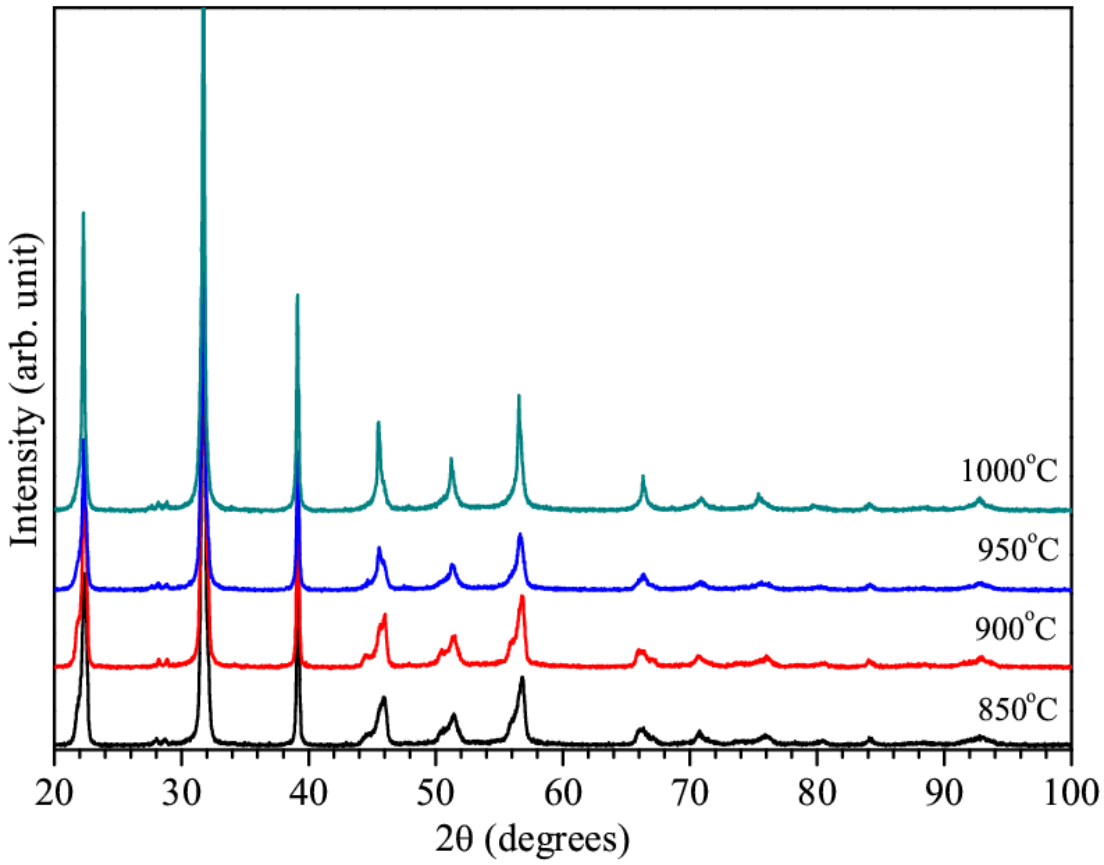

Fig.3.10 Powder XRD patterns of 0.65BMT-0.35PT piezoceramics with heat treatment temperature.

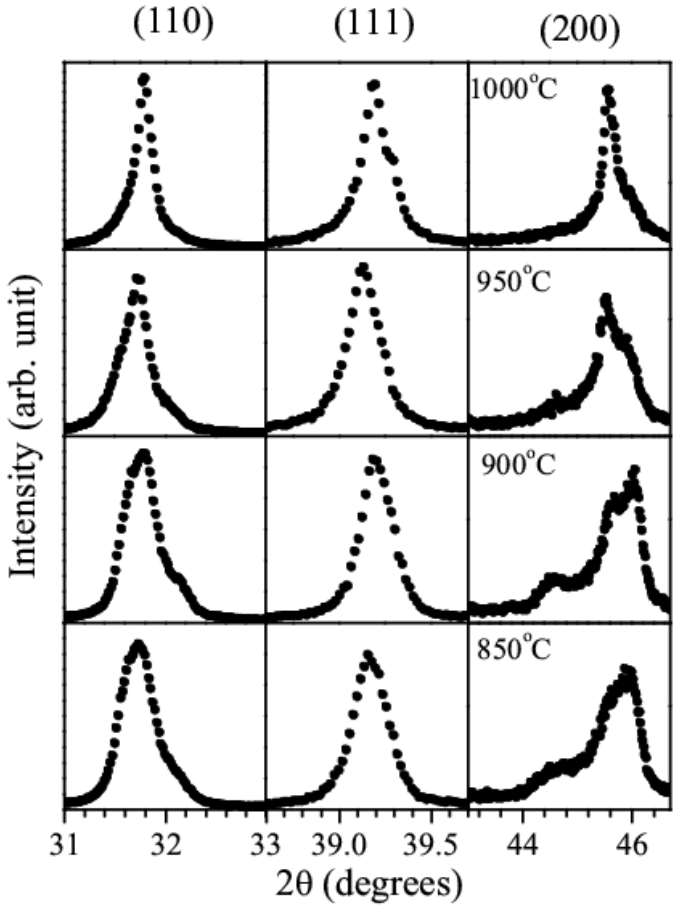

Fig.3.11 Evolution of XRD profiles for pseudocubic (110), (111) and (200) reflections of 0.65BMT-0.35PT piezoceramics with heat treatment temperature.

3.6.2 Rietveld analysis of XRD data with heat treatment temperature

As discussed in forgoing sections, the structure of the composition with x=0.35, after sintering at 950^{o}C is coexistence of tetragonal and monoclinic phases. The Rietveld structural analysis of the samples heat treated at various temperature also reveals coexistence of (Pm+T) phases for all the samples. Fig.3.12 shows the Rietveld fits for the pseudocubic (110), (111), and (200) profiles, for the composition with x=0.35, using coexisting "Pm+P4mm" structures, for the samples heat treated at 850^{o}C, 900^{o}C, 950^{o}C, and 1000^{o}C. The structure of all the samples can be fitted well by considering coexistence of the monoclinic (Pm) and tetragonal (P4mm) structures. Rietveld analysis confirms that the phase stability of the two coexisting phases is being altered by heat treatment temperature.

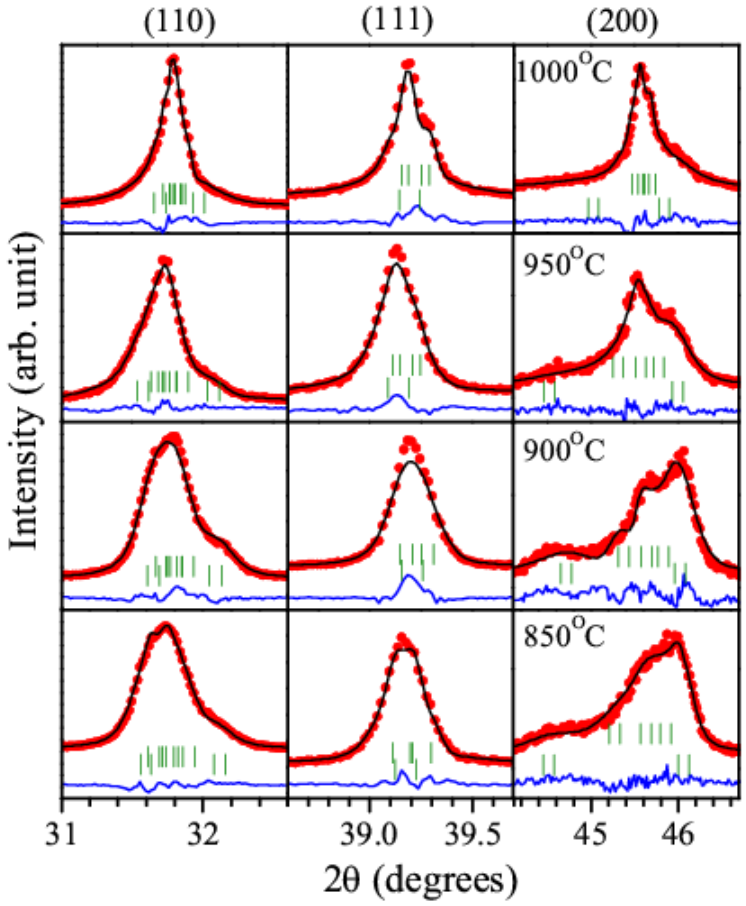

Fig.3.12 Experimentally observed (dots), Rietveld calculated (continuous line), and their difference (continuous bottom line) profiles for pseudocubic (110), (111) and (200) reflections obtained after Rietveld analysis of XRD data for 0.65BMT-0.35PT using coexistence monoclinic+tetragonal (Pm+P4mm) structures for samples heat treated at various temperatures. The vertical tick marks above the bottom line show peak position.

3.6.3 Variation of lattice parameters and monoclinic phase fraction with composition

The variation of lattice parameters with heat treatment temperature for BMT-PT for the composition x=0.35 is shown in Fig. 3.13. The lattice parameters of monoclinic phase are denoted by a_M, b_M, and c_M. The monoclinic angle is denoted by β. The lattice parameters of tetragonal phase are denoted by a_T and c_T. As shown in Fig. 3.13, the monoclinic a_M and b_M parameters are almost constant with increasing heat treatment temperature but the "c_M" and monoclinic angle β parameter shows slightly increasing trend. The tetragonal a_T parameter decreases, while the c_T parameter increases continuously with increasing the heat treatment temperature. Thus, even though, the cell parameters of the two coexisting phases are showing slight variation with heat treatment temperature. The relative phase fractions are being altered significantly. Variation of the monoclinic phase fraction with heat treatment temperature, for the composition x=0.35, is shown in Fig. 3.14. The fraction of monoclinic phase linearly decreases with heat treatment temperature. Increasing heat treatment temperature stabilizes more tetragonal phase at the expense of the monoclinic phase. The fraction of monoclinic phase is 79.06% for the sample heat treated at 850^{o}C, which decreases to 48.34% for the sample heat treated at 1000^{o}C.

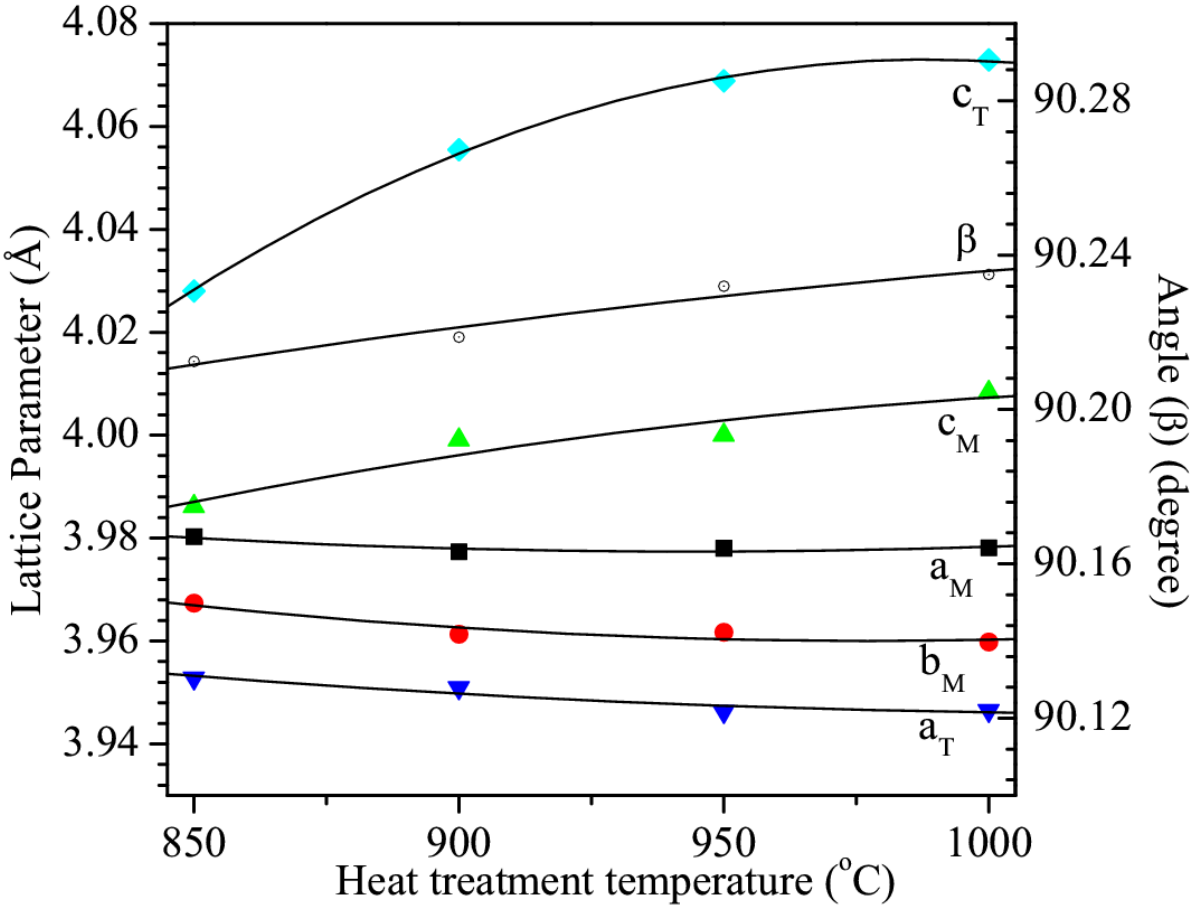

Fig.3.13 Variation of lattice parameters with heat treatment temperature for 0.65BMT-0.35PT.

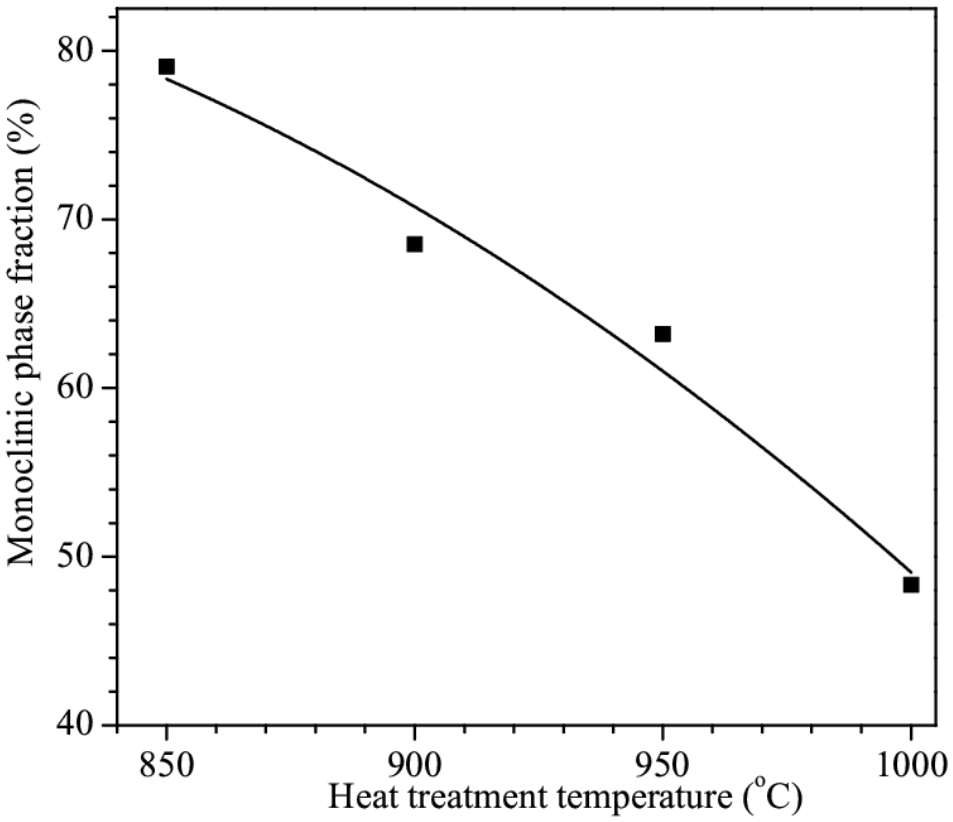

Fig.3.14 Variation of monoclinic phase fraction with heat treatment temperature for 0.65BMT-0.35PT.

Recently, it has been reported for $0.71BiFeO_3$-$0.29PbTiO_3$ also that tetragonal phase transforms to coexisting tetragonal and rhombohedral phases on reducing crystallite size [Kothai et al. (2014)]. Since the grain size of the BMT-PT samples prepared at lower temperature will be smaller, it is expected that they will have more monoclinic phase.

3.6.4 Microstructure studies

We studied the microstructure of these samples using scanning electron microscopy (SEM) to confirm that the varying phase stability with heat treatment temperature is linked with the grain size. The SEM images of BMT-PT (x=0.35) samples for the heat treatment temperatures 850^{o}C, 900^{o}C, 950^{o}C, and 1000^{o}C are shown in Figs. 3.15(a)-(d) respectively. The average grain size for the sample heat treated at 850^{o}C is 200nm, which increases to ~400nm for sample heat treated at 900^{o}C. The average grain size for the sample heat treated at 950^{o}C is in between 0.5 and 1µm. The grain size increases further for the sample heat treated at 1000^{o}C. The sizes of the most of the grains are in between 1.5 and 2µm. As expected, the grain size is continuously increasing with increasing heat treatment temperature. This suggests that the bigger grain size is favouring stability of tetragonal structure, while the smaller grain size favours the stability of the monoclinic structure. It is shown for $PbTiO_3$ that a monoclinic phase can appear when the material is kept under high pressure. In our samples, decreasing the grain size may result into similar condition but the external pressure is arising from the excess surface energy. For the smaller grain size, surface to volume ratio is high so that grains are having more surface energy. The excess surface

energy may translate as external pressure applied to the system and can stabilize the monoclinic phase. If one prepares these samples, by different synthesis methods under different heat treatment conditions, the obtained grain size of the samples will be different. Depending upon the grain size, the observed crystal structure will be predominantly monoclinic (rhombohedral) or tetragonal for the compositions around MPB where phase stability is sensitive to small changes in composition and temperature. This is the reason why some researchers have reported rhombohedral structure [Randall et al. (2004); Zhang et al. (2011)] for BMT-PT (x=0.35), while some researchers have reported coexistence of the rhombohedral and tetragonal phases [Chen et al. (2009); Zhang et al. (2010)]. The varying phase coexistence region in BMT-PT is also reported by various authors [Randall et al. (2004); Zhang et al. (2011)] in the samples prepared by different methods.

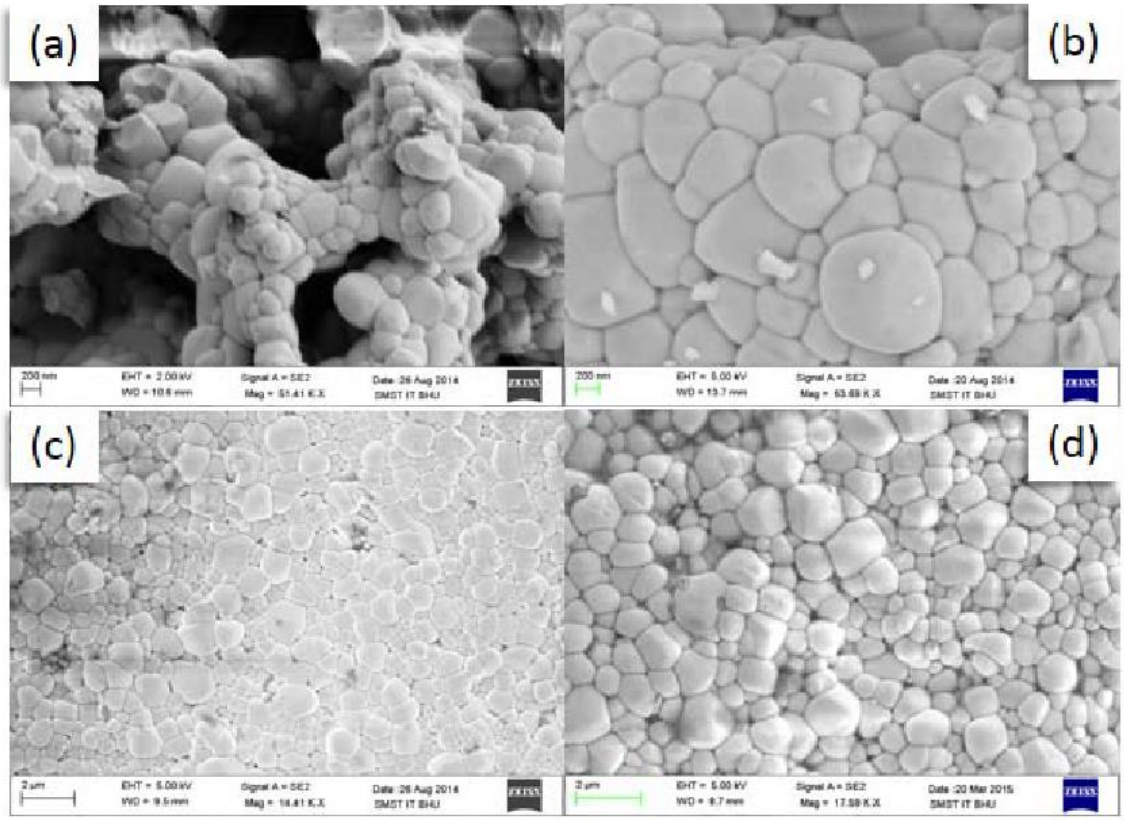

Fig.3.15 SEM images of 0.65BMT-0.35PT ceramics, heat treated at temperatures (a) 850^{o}C, (b) 900^{o}C, (c) 950^{o}C, and (d) 1000^{o}C.

3.7 Crystal structure and location of MPB in BMZ-PT at room temperature

The BMZ-PT solid solution is completely different from BMT-PT system. The BMZ-PT has very narrow ($\Delta x=0.03$) compositional width of the MPB region while it is much wider ($\Delta x=0.08$) for BMT-PT system. The room temperature powder x-ray diffraction patterns of the BMZ-PT ceramics sintered at 975^{o}C with x=0.55, 0.56, 0.57, 0.58, 0.59 and 0.60 collected for the two-theta range of 20^{o}-60^{o} is shown in Fig. 3.16. All the reflections shown in Fig. 3.16 correspond to perovskite structure except negligibly weak reflections (marked with asterisks) around two-theta ~27.58^{o}, 28.69^{o} and 32.82^{o} in the XRD profile. Similar impurity reflections are present in the XRD patterns of BMZ-PT samples reported by earlier workers [Shabbir et al. (2007); Qureshi et al. (2007)]. Eliminating these impurity phases requires multiple calcination and sintering steps [Suchomel et al. (2004)]. Our samples were prepared in a single-step calcination and sintering schedule. The phase fraction for this impurity phase is negligibly small, as determined by the Rietveld method. A careful examination of Fig. 3.16 suggests the presence of three different crystallographic compositional regions: $x>0.59$, $x<0.57$, and $0.57\leq x\leq 0.59$, where the nature of the XRD profiles changes (see e.g. the peak around two-theta = 46^{o} encircled in Fig. 3.16). To analyse the structure, we have shown in Fig. 3.17 the selected pseudo-cubic (110), (111) and (200) profiles of BMZ-PT ceramics with x=0.55, 0.56, 0.57, 0.58, 0.59 and 0.60. The contribution from the $CuK_{\alpha 2}$ wavelength has been subtracted by using standard software, for all the profiles shown in Fig. 3.17.

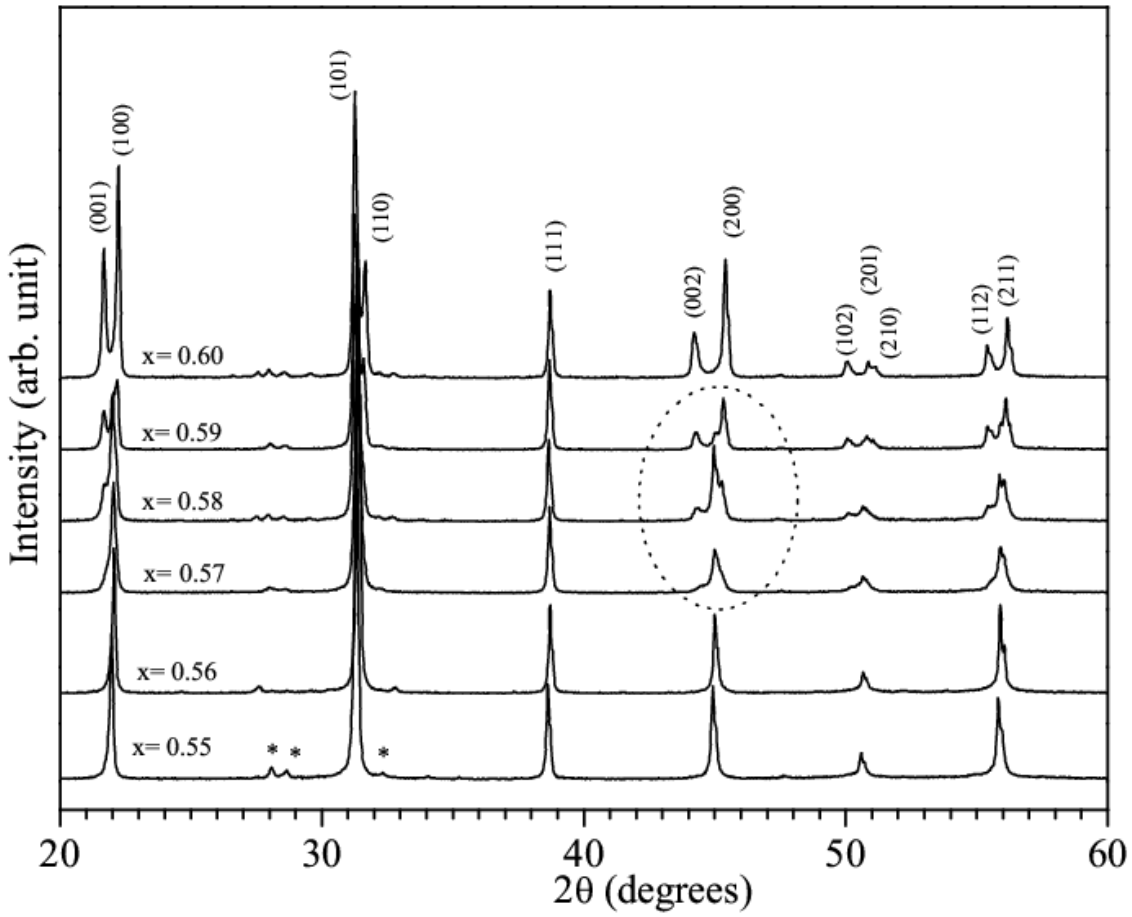

Fig.3.16 Powder XRD patterns of (1-x)Bi($Mg_{1/2}Zr_{1/2}$)O_3-x$PbTiO_3$ ceramics with x=0.55, 0.56, 0.57, 0.58, 0.59 and 0.60 sintered at 975^{o}C. Weak reflections marked by asterisks are due to the impurity phase. Miller indices are given using tetragonal structure for x=0.60.

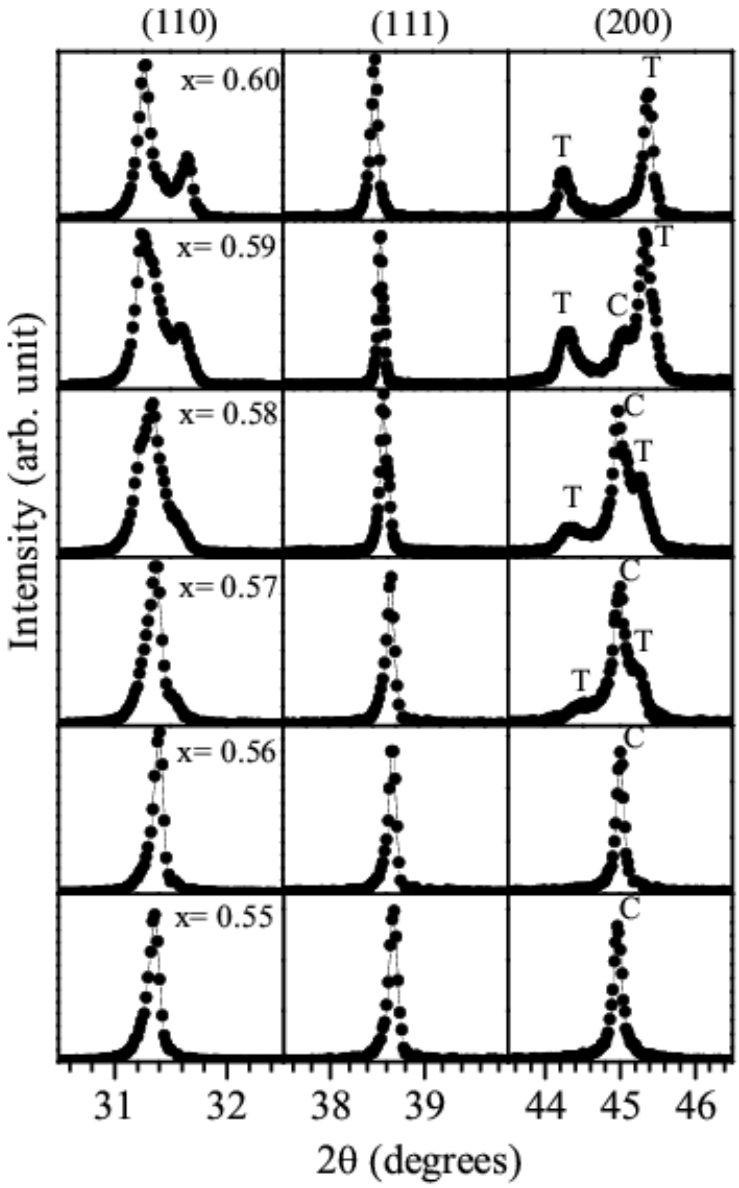

Fig.3.17 Pseudocubic (110), (111) and (200) powder XRD profiles of (1-x)Bi($Mg_{1/2}Zr_{1/2}$)O_3-x$PbTiO_3$ ceramics for the compositions with x=0.55, 0.56, 0.57, 0.58, 0.59 and 0.60. The peaks marked with "C" and "T" correspond to cubic and tetragonal phases, respectively.

All the pseudo-cubic reflections shown in Fig. 3.17 appear to be singlet for the compositions with $x \leq 0.56$. This characterizes a cubic structure with space group Pm3m for the compositions with $x \leq 0.56$. This is consistent with the results of Suchomel and Davies (2004), where cubic structure is reported for x=0.55. The (110) and (200) profiles are clearly split into doublets while the (111) profile remains singlet for the composition with x=0.60. This characterizes the tetragonal structure for $x \geq 0.60$. Earlier authors have also reported a tetragonal structure with space group P4mm for x=0.60 [Suchomel et al. (2004); Shabbir et el. (2007)]. For the compositions with x=0.57, 0.58 and 0.59, the examination of the (200) pseudocubic XRD profile shown in Fig. 3.17 suggests that the peaks corresponding to both the cubic and tetragonal phases are present, indicating the coexistence of these two phases. Thus the compositions with $0.57 \leq x \leq 0.59$ correspond to the MPB region in which both the tetragonal and cubic phases coexist. As shown in Fig. 3.17, the intensity of the peak corresponding to the cubic phase marked by "C" is dominant in x=0.57 and 0.58 while the intensity of the peak corresponding to the tetragonal phase marked by "T" is dominant in x=0.59. There is no lower angle splitting or asymmetry in the (111) profile expected for the rhombohedral/monoclinic structures. This suggests that the rhombohedral structure is not present in or outside the MPB region in BMZ-PT ceramics. To confirm the structure of these compositions we have carried out Rietveld structural analysis of the powder XRD patterns for these samples. The results are resented in subsequent sections.

3.7.1 Rietveld analysis of x-ray powder diffraction data

In this Section, we present the results of Rietveld analysis for the confirmation of the crystal structure of BMZ-PT solid solutions across the MPB region. The Rietveld structure refinement for all the compositions has been carried out to determine precisely the structural parameters. The Rietveld fits for x=0.56, 0.59 and x=0.60 using cubic, cubic+tetragonal and tetragonal structures, respectively, are shown in Fig. 3.18, 3.19, and 3.20 respectively.

3.7.1.1 Cubic structure with space group Pm3m (x<0.57)

As discussed in Section 3.7, the XRD profiles for the composition with x<0.57 do not show any splitting and appear to be singlet. We have refined the structure of these compositions using cubic phase with space group Pm3m. Fig. 3.18 depicts the Rietveld fit of the XRD data for x=0.56 using the cubic space group Pm3m. The fit between the observed and calculated profiles is quite good, confirming the cubic structure of BMZ-PT for x<0.57. The inset shows the goodness of fit for the pseudocubic (111) profile. It is clear from inset of Fig.3.18 that (111) profile is a singlet and no asymmetry or splitting is observed in lower two-theta side. For rhombohedral phase of other MPB systems like PZT [Noheda et al. (1999)], PMN-PT [Singh et al. (2001), (2003), (2007)] etc. a lower angle peak or asymmetric tail is clearly observed due to splitting of (111) profile into a doublet. Thus the structure of BMZ-PT compositions with x<0.57 is cubic in the Pm3m space group.

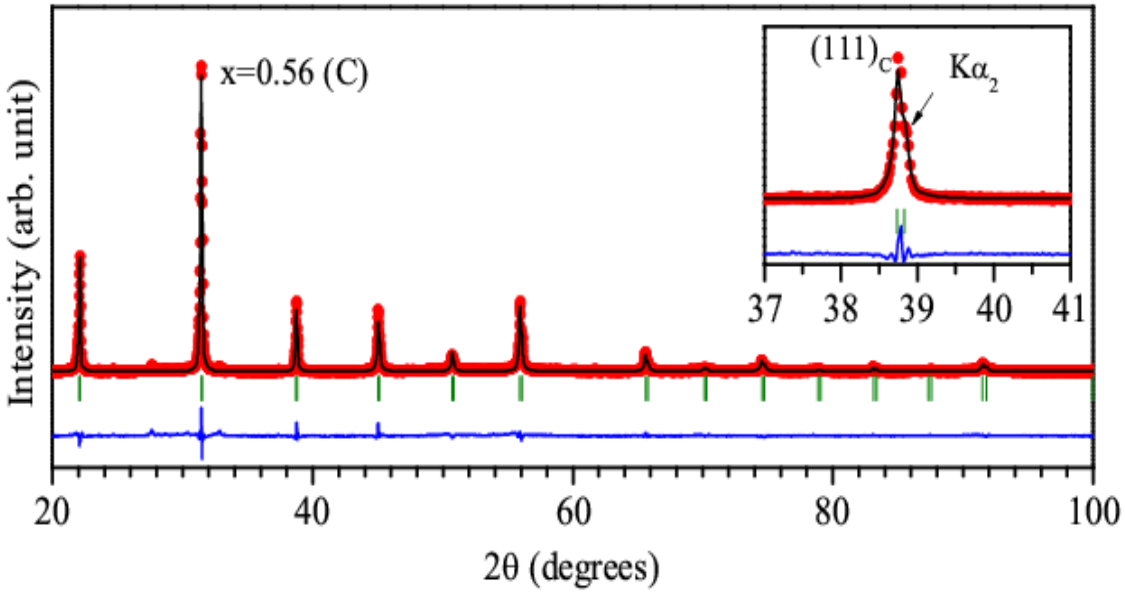

Fig.3.18 Experimentally observed (dots), Rietveld calculated (continuous line) and their difference (continuous bottom line) profiles for (1-x)Bi($Mg_{1/2}Zr_{1/2}$)O_3-x$PbTiO_3$ with x=0.56 obtained after Rietveld analysis of the powder XRD data using cubic (Pm3m) structure. The vertical tick marks above the difference plot show the peak positions. The insets illustrate the goodness of fit.

3.7.1.2 Phase coexistence with space groups Pm3m+P4mm (0.57≤x≤0.59)

To confirm the phase coexistence of tetragonal and cubic phases and for the sake of completeness, we have analyzed the crystal structure of MPB compositions ($0.57 \leq x \leq 0.59$, $\Delta x=0.03$) using various plausible structures, i.e. rhombohedral (R3m), cubic (Pm3m) and monoclinic (Pm and Cm) coexisting with the tetragonal (P4mm) structure. Our Rietveld analysis of the XRD data for these compositions reveals that the best fit is obtained for the coexistence of cubic and tetragonal (Pm3m+P4mm) phases. The value of $\chi^2=2.19$ is also a minimum for this structural model as against the (R3m+P4mm) model giving $\chi^2=3.80$ for x=0.59. Fig. 3.19 shows very good Rietveld fit for the composition with x=0.59 using coexisting cubic and tetragonal structure. A comparison of the (C+T) and (R+T) phase coexistence models suggests that the refined lattice parameters for the tetragonal phase were same in both the models. In the R+T model, the refined lattice parameters for the hexagonal unit cell (space group R3mH) are obtained as $a_H=b_H=5.685(1)$ Å, $c_H=6.9715(2)$ Å. For a direct comparison with the lattice parameter of the cubic phase in the C+T model, the rhombohedral lattice parameters (a_R,α_R) were calculated by using hexagonal unit cell parameters (a_H, c_H) according to Eqs. (3.1) and (3.2) as shown in Ref. [Hahn (2006)].

$$a_R=\frac{1}{3}\sqrt{(3a_H^2+c_H^2)} \quad \ldots\ldots\ldots\ldots\ldots\ldots \quad 3.1$$

$$\cos(\alpha_R)=\frac{(2c_H^2-3a_H^2)}{(2c_H^2+6a_H^2)} \quad \ldots\ldots\ldots\ldots\ldots\ldots \quad 3.2$$

The value of the rhombohedral lattice parameter a_R=4.0219(1) Å is comparable to the cubic lattice parameter (a_C=4.0191(2) Å) for the C+T model. The value of the rhombohedral angle comes out to be a_R=89.95(5) degree, which may be considered as 90^o taking into account the standard deviation. Thus, we may conclude that the structure of BMZ-PT for the compositions with $0.57 \leq x \leq 0.59$ consists of coexisting cubic and tetragonal phases (Pm3m+P4mm) and not the rhombohedral and tetragonal (R3m+P4mm) phases as reported earlier [Shabbir et al. (2007); Qureshi et al. (2007)]. This is further confirmed by the absence of splitting in the (111) pseudo-cubic XRD profiles expected for the rhombohedral structure (see Fig. 3.19 and inset to Fig. 3.19). In contrast, the MPB systems such as PZT [Pandey et al. (2008)] and PMN-PT [Singh et al. (2003), (2006)] show clear splitting in the (111) pseudo-cubic XRD profile for the compositions with rhombohedral structure. First-principles density functional calculations by Grinberg and Rappe (2007) also suggest that T_C decreases rapidly for BMZ-PT solid solution with decreasing PT concentration and approaches 300K for x~0.50. The refined structural parameters and the agreement factors are listed in Table 3.4 for $0.57 \leq x \leq 0.59$ using the coexistence of tetragonal (P4mm) and cubic (Pm3m) phases.

Table 3.4: Refined structural parameters and agreement factors for BMZ-PT ceramics with x=0.59 using coexisting cubic (Pm3m)+tetragonal (P4mm) structures.

x (space group)	Ions	x	y	z	Thermal parameters (Å^2)	Lattice Parameters (Å)
0.59	Bi/Pb	0.0	0.0	0.0	Biso=4.6(1)	a_C=4.0191(2)
(Pm3m)	Mg/Zr/Ti	0.5)	0.5	0.5	Biso=2.3(2)	
	O	0.5	0.5	0.0	Biso=6.0(9)	
(P4mm)	Bi/Pb	0.0	0.0	0.0	$\beta_{11}=\beta_{22}$=0.071(1),	a_T=3.9909(1)
					β_{33}=0.034(2)	c_T=4.0801(2)
	Mg/Zr/Ti	0.5	0.5	0.546(1)	Biso=0.2(1)	
	O_I	0.5	0.5	0.10(6)	Biso=2.6(6)	
	O_{II}	0.5	0.0	0.615(2)	Biso=0.4(3)	

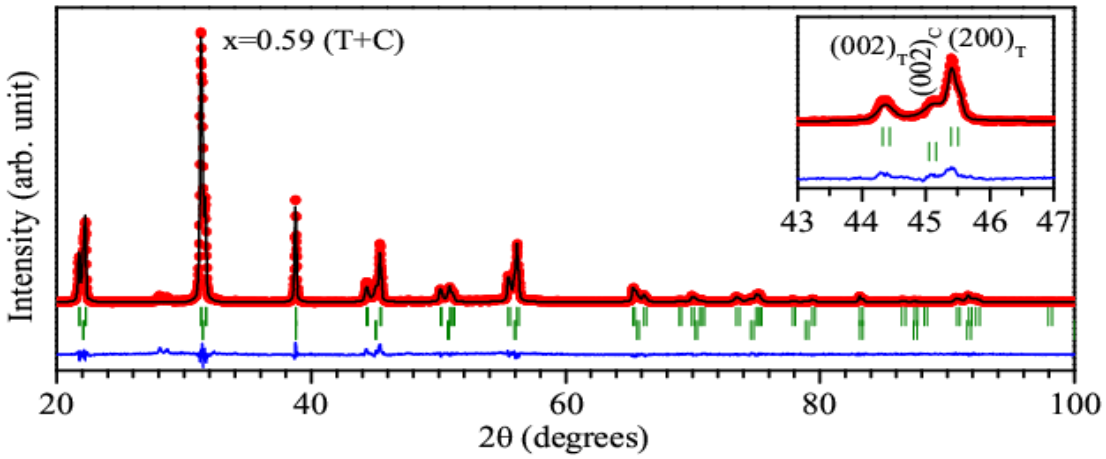

Fig.3.19 Experimentally observed (dots), Rietveld calculated (continuous line) and their difference (continuous bottom line) profiles for (1-x)Bi($Mg_{1/2}Zr_{1/2}$)O_3-x$PbTiO_3$ with x=0.59 obtained after Rietveld analysis of the powder XRD data using tetragonal+cubic (P4mm+Pm3m) structures. The vertical tick marks above the difference plot show the peak positions. The inset illustrates the goodness of fit.

3.7.1.3 Tetragonal structure with space group P4mm (x≥0.60)

As discussed in Section 3.7, the BMZ-PT for the compositions with x≥0.60 exhibit well resolved doublets for (110) and (200) profiles, while the (111) profile is a singlet characterising tetragonal structure for this composition similar to the end component $PbTiO_3$. The Rietveld analysis also confirms the tetragonal structure with space group P4mm for x=0.60 is shown in Fig.3.20. Very good fits between the observed and Rietveld calculated profiles were obtained by using the tetragonal P4mm space group. The consideration of small coexisting cubic phase (for x=0.60) further improves the fit; however, the structure is predominantly tetragonal. The refined structural parameters and the agreement factors are listed in Table 3.5 for x≥0.60 using the tetragonal (space group P4mm) structure.

Table 3.5: Refined structural parameters and agreement factors for BMZ-PT ceramics with x=0.60 using tetragonal (P4mm) structures.

x (space group)	Ions	x	y	z	Thermal parameters (Å^2)	Lattice Parameters (Å)
0.60 (P4mm)	Bi/Pb	0.0	0.0	0.0	$\beta_{11}=\beta_{22}=0.049(1)$, $\beta_{33}=0.017(1)$	$a_T=3.9886(2)$ $c_T=4.0834(2)$
	Mg/Zr/Ti	0.5	0.5	0.55(1)	$B_{iso}=0.22(8)$	
	O_I	0.5	0.5	0.082(4)	$B_{iso}=1.2$ (6)	
	O_{II}	0.5	0.0	0.61(3)	$B_{iso}=0.0(3)$	

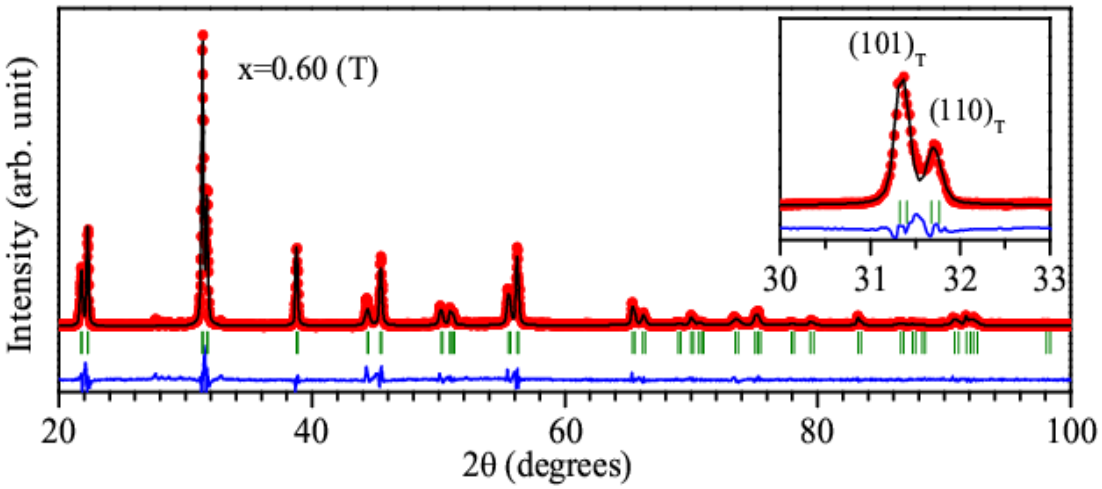

Fig.3.20 Experimentally observed (dots), Rietveld calculated (continuous line) and their difference (continuous bottom line) profiles for (1-x)Bi($Mg_{1/2}Zr_{1/2}$)O_3-x$PbTiO_3$ with x=0.60 obtained after Rietveld analysis of the powder XRD data using tetragonal (P4mm) structure. The vertical tick marks above the difference plot show the peak positions. The inset illustrate the goodness of fit.

3.7.2 Variation of lattice parameters and tetragonal phase fraction with composition

Variations of the tetragonal phase fraction and lattice parameters with composition, as obtained by Rietveld refinement of the structure, are plotted in Fig. 3.21. It is evident from this figure that a very small change in PT concentration (x) affects significantly the fraction of the tetragonal phase. As is expected, the tetragonality increases with increasing PT concentration for the tetragonal phase region. The values of the lattice parameters for x=0.55 and 0.60 are in good agreement with those reported by Suchomel and Davies (2004).

3.8 Discussions

Recent developments in theoretical and experimental research have improved our understanding towards the phase stabilities in the vicinity of MPB based $Pb(Zr_xTi_{1-x})O_3$ (PZT) [Jaffe et al. (1971)] and PMN-PT solid solutions [Park et al. (1997)]. As discussed in Chapter 1, the structure of the PZT below room temperature has been revisited by Noheda et al. (2000) and they discovered a new phase transition from the room temperature tetragonal phase to a monoclinic phases in Cm space group for the composition x=0.50, and 0.52 close to MPB composition below room temperature [Noheda et al., (2000), (2006); Ragini et al. (2001)]. One more phase transition from monoclinic phase with space group Cm to another monoclinic phase with space group Cc is discovered at low temperatures in PZT, which is antiferrodistortive (AFD) transition [Hatch et al. (2002)]. The AFD transition leads to superlattice reflections which is observed in neutron and electron diffraction only [Ragini et al. (2001)].

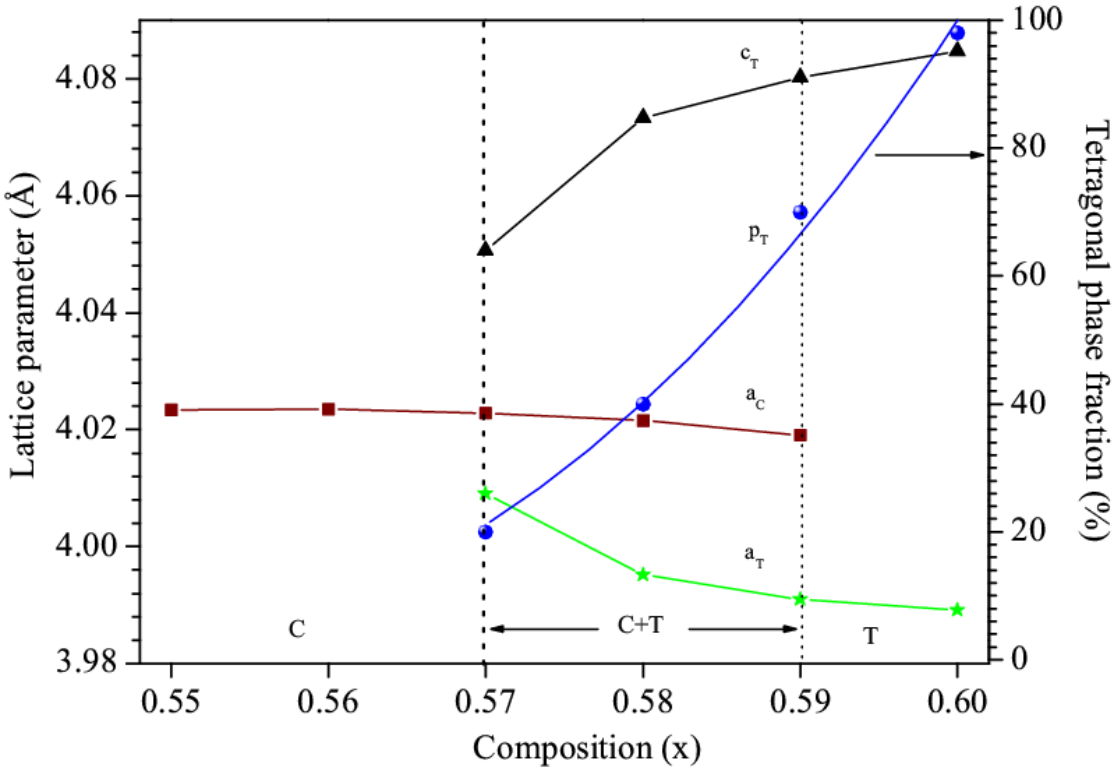

Fig.3.21 Compositional variation of cubic (a_C), tetragonal (a_T, c_T) lattice parameters and tetragonal phase fraction (P_T) for (1-x)$Bi(Mg_{1/2}Zr_{1/2})O_3$-x$PbTiO_3$ ceramic a cross MPB obtained after Rietveld analysis. Continuous lines are guides for the eyes.

The monoclinic phase with space group Cm provides the path for the rotation of polarization vector between tetragonal (space group P4mm) and rhombohedral (space group R3m) structure. Similar to PZT, the presence of monoclinic phase is observed in $Pb(Mg_{1/3}Nb_{2/3})O_3$-$xPbTiO_3$ [PMN-PT] with space group Pm in the morphotropic phase boundary region at room temperature [Singh et al. (2003)]. Another monoclinic phase with space group Cm is also observed in the morphotropic phase boundary region of PMN-PT solid solution [Singh et al. (2003)].

The results discussed in the preceding sections confirm that the structure of the MPB region for BMT-PT piezoceramics is monoclinic with space group Pm, while there is no monoclinic phase in BMZ-PT piezoceramics. Vanderbilt and Cohen (2001) explained the stability of monoclinic phases in ferroelectric perovskites by considering eighth coefficient free energy in the expansion of Landau-Devonshire (LD) theory of ferroelectric homogeneous state [Vanderbilt et al. (2001)]. In case of BMZ-PT piezoceramics the structure of the MPB phase is the coexistence of cubic and tetragonal phase. Noheda et al. (1999) discovered a monoclinic phase in the PZT system. The monoclinic phases is observed in several other MPB solid solutions such as PMN-PT [Singh et al. (2001), (2003)], PZN-PT [Orauttapong et al. (2002)], BNT-PT [Pandey and Singh (2014)], BS-PT [Chaigneau et al. (2007)] etc. Fu and Cohen (2000) have shown that the first principles calculations for the rotation of polarization vector, in planes corresponding to the monoclinic phases observed in the MPB region. The

polarization vector has more freedom to rotate in the monoclinic phase in comparison to the coexisting rhombohedral and tetragonal phases.

Similar to BMZ-PT, the coexistence of the cubic and tetragonal phases is observed in the MPB region for the (1-x)$Pb(Fe_{2/3}W_{1/3})O_3$-x$PbTiO_3$ ceramics, but the phase coexistence region ($0.20 \leq x \leq 0.37$) is very wide [Mitoseriu et al. (2002), (2003)]. The compositional width of the MPB is very narrow in the BMZ-PT system, similar to PZT [Noheda et al. (1999)]. The fact that some MPB systems such as PZT [Pandey et al. (2008)], BS-PT [Eitel et al. (2001), (2002); Chaigneau et al. (2007); Alguero et al. (2012)], BF-PT [Bhattacharjee et al. (2007)] and BMZ-PT have a very narrow compositional width of the phase coexistence region while the MPB systems such as PMN-PT [Singh et. al. (2003), (2006)], BMT-PT [Randall et al. (2004)]and (1-x)$Pb(Fe_{2/3}W_{1/3})O_3$-xPbTiO3 [Mitoseriu et al. (2002), (2003)] have a wide phase coexistence region is highly intriguing. Suchomel and Davies (2004) have successfully correlated the position and compositional width of the phase coexistence region for the MPB ceramics with the tolerance factor. It has been reported that the position of the MPB shifts to the $PbTiO_3$ rich end as the difference of the tolerance factor with the other end component increases. However, an increase in the difference of the tolerance factor results in a narrow compositional width of the MPB. This is indeed the case for the MPB ceramics such as PZT [Pandey et al. (2008)] and BS-PT [Eitel et al. (2001), (2002); Chaigneau et al. (2007); Alguero et al. (2012)] as well as for the BMZ-PT system. BF-PT [Bhattacharjee et al. (2007)] may be an exception for which the MPB lies on the lower PT side, while the compositional

width of the MPB is also narrow. The presence of rotational instabilities in the rhombohedral structure of $BiFeO_3$ may be a reason for this anomaly [Bhattacharjee et al. (2007)]. More detailed theoretical studies will help to understand the location and the compositional width of the MPB in lead and bismuth based MPB systems. Further, in the PMN-PT system the structure of the component PMN is pseudo-cubic but in the vicinity of the MPB, short range monoclinic followed by a long range monoclinic structure is stabilized with $PbTiO_3$ substitution [Singh et. al. (2003), (2006)]. Theoretical studies will help to understand why a similar rhombohedral/monoclinic phase is not stabilized in the vicinity of the MPB in the BMZ-PT system. As observed in a number of lead based piezoceramics [Singh et. al. (2003), (2006)], the isotropic thermal parameters of the A-site cations (Pb^{2+}/Bi^{3+}) were very high (>4Å^2). In view of this we considered anisotropic thermal parameters for these ions in tetragonal structure. The thermal ellipsoid is more elongated about the xy-axes than the z-axis. For the cubic phase of the x=0.59 composition, the refined thermal parameters for oxygen and B-site cations ($Mg^{2+}/Zr^{4+}/Ti^{4+}$) were also very high. However, fixing their values to a low level manually does not affect significantly the value of χ^2, suggesting that these parameters are not correctly determined with the XRD data. Powder neutron diffraction data will be needed to ascertain correctly the thermal parameters for these ions.

3.9 Conclusions

Rietveld structure refinement of various compositions of BMT-PT across MPB reveals a monoclinic structure in Pm space group for the compositions with

$x \leq 0.32$. The structure is tetragonal with space group P4mm for the compositions $x > 0.40$. Coexistence of monoclinic (Pm) and tetragonal (P4mm) structures is observed for the MPB region in the composition range $0.33 \leq x \leq 0.40$. Phase stability is found to be strongly correlated with the grain size in the MPB region. Increasing heat treatment temperature in BMT-PT piezoceramics, increases the grain size and phase fraction of the tetragonal phase in the coexistence region.

Detailed Rietveld analysis of the structure of BMZ-PT for the compositions with $0.55 \leq x \leq 0.60$ reveals that the structure is cubic in the Pm3m space group for the compositions with $x < 0.57$, tetragonal in the space group P4mm for the compositions with $x > 0.59$ while the two phases coexist for the intermediate compositions. Thus the width of the MPB region is very narrow, $\Delta x \sim 0.03$. Our results clearly rule out the coexistence of tetragonal and rhombohedral structures for the MPB compositions, as reported earlier for BMT-PT and BMZ-PT piezoceramics.